SEDIMENTOLOGY the journal of the International Association of Sedimentologists

Sedimentology (2020) **67**, 3259–3289 doi: 10.1111/sed.12746

Stratigraphic hierarchy and three-dimensional evolution of an exhumed submarine slope channel system

DANIEL BELL*† , DAVID M. HODGSON‡, ANNA S. M. PONTÉN§, LARISSA A. S. HANSEN‡, STEPHEN S. FLINT* and IAN A. KANE*

**School of Earth and Environmental Sciences, University of Manchester, Oxford Road, Manchester, M139PL, UK (E-mail: daniel.bell1@ucalgary.ca)*

†Department of Geoscience, University of Calgary, Calgary, Alberta, T2N 1N4, Canada

‡Stratigraphy Group, School of Earth and Environment, University of Leeds, Leeds, LS2 9JT, UK

§Research Centre Rotvoll, Equinor ASA, NO-7005, Trondheim, Norway

Associate Editor – Jaco Baas

ABSTRACT

Submarine slope channel systems have complicated three-dimensional geometries and facies distributions, which are challenging to resolve using subsurface data. Outcrop analogues can provide sub-seismic-scale detail, although most exhumed systems only afford two-dimensional constraints on the depositional architecture. A rare example of an accessible fine-grained slope channel complex set situated in a tectonically quiescent basin that offers seismic-scale, down-dip and across-strike exposures is the Klein Hangklip area, Tanqua-Karoo Basin, South Africa. This study investigates the three-dimensional architecture of this channel complex set to characterise the stratigraphic evolution of a submarine channel-fill and the implications this has for both sediment transport to the deep-oceans and reservoir quality distribution. Correlated sedimentary logs and mapping of key surfaces across a 3 km^2 area reveal that: (i) the oldest channel elements in channel complexes infill relatively deep channel cuts and have low aspect-ratios. Later channel elements are bound by comparatively flat erosion surfaces and have high aspect-ratios; (ii) facies changes across depositional strike are consistent and predictable; conversely, facies change in successive down depositional dip positions indicating longitudinal variability in depositional processes; (iii) stratigraphic architecture is consistent and predictable at seismic-scale both down-dip and across-strike in three-dimensions; (iv) channel-base-deposits exhibit spatial heterogeneity on one to hundreds of metres length-scales, which can inhibit accurate recognition and interpretations drawn from one-dimensional or limited two-dimensional datasets; and (v) channel-base-deposit character is linked to sediment bypass magnitude and longevity, which suggests that time-partitioning is biased towards conduit excavation and maintenance rather than the fill-phase. The data provide insights into the stratigraphic evolution and architecture of slope channel-fills on fine-grained continental margins and can be utilised to improve predictions derived from lower resolution and one-dimensional well data.

Keywords Channel architecture, channel base drape, channel hierarchy, Karoo Basin, sediment bypass, submarine channel.

INTRODUCTION

Submarine slope channels are conduits for some of the largest sediment transport events on Earth (e.g. Piper & Aksu, 1987; Gonzalez-Yajimovich *et al.,* 2007; Talling *et al.,* 2007; Jobe *et al.,* 2018), with individual flows up to an order of magnitude larger than the global annual flux of rivers to the ocean (Milliman & Syvitski, 1992; Talling *et al.*, 2007; Sømme *et al.*, 2009). Submarine gravity flows within these channels transport large quantities of organic carbon and anthropogenic pollutants to their ultimate sink on the basin-floor (Galy *et al.,* 2007; Gwiazda *et al.,* 2015; Kane & Clare, 2019). Additionally, slope channel-fills can act as valuable archives of past climatic and tectonic events (e.g. Mutti, 1984; Bruhn & Walker, 1997; Clark & Cartwright, 2009; Pickering & Bayliss, 2009; Covault & Graham, 2010; Hirst, 2012; Scotchman *et al.,* 2015; Castelltort *et al.,* 2017) and form important hydrocarbon reservoirs on continental margins around the world (Bruhn & Walker, 1997; Weimer *et al.*, 2000; Kolla *et al.*, 2001; Prather, 2003; Mayall *et al.*, 2006; Zhang *et al.*, 2015).

The evolution and character of slope channels is challenging to decipher using subsurface data, as they are often characterised by complicated three-dimensional (3D) facies heterogeneity and depositional geometries at sub-seismic scale. Outcrop analogues can help to bridge this scale gap and provide data to populate 3D bodies mapped in seismic with stratigraphic and facies information (e.g. Bryant & Flint, 1992; Clark & Pickering, 1996; Campion *et al.,* 2000; Sullivan *et al.,* 2000; McCaffrey & Kneller, 2001; Hodgetts *et al.,* 2004; Bakke *et al.,* 2008, 2013; Hofstra *et al.,* 2017). Most outcrops only afford two-dimensional (2D) constraints of the depositional architecture, which provides only limited information on how architecture and facies vary either laterally (across-strike) or longitudinally (down-dip) (e.g. Walker, 1966a, 1966b, 1975; Campion *et al.*, 2000; Sullivan *et al.*, 2000; Schwarz & Arnott, 2007; Kane *et al.*, 2009; Moody *et al.*, 2012; Macauley & Hubbard, 2013; Bain & Hubbard, 2016; Li *et al.*, 2016; Morris *et al.*, 2016; Pitts *et al.*, 2017). Few outcrop-based studies have been able to investigate the 3D architecture and stratigraphic evolution of submarine channel-fills and those that do rely on extrapolation of LiDAR (light detection and ranging) data from oblique sections (Pyles *et al.,* 2010, 2012). Additionally, most outcrop analogues are from relatively small foreland basins, with small catchments and coarse-grained sediment (Beaubouef, 2004; De Ruig & Hubbard, 2006; Jobe *et al.*, 2010; Moody *et al.*, 2012; Hubbard *et al.*, 2014; Bain & Hubbard, 2016; Casciano *et al.*, 2019), which are poor analogues for the comparatively large, fine-grained and mud-rich systems that are common in offshore passive margin settings with large drainage basins (e.g. Reading & Richards, 1994; Bouma, 2000; Stelting *et al.,* 2000; Hubbard *et al.,* 2005; Pickering & Corregidor, 2005; Prélat *et al.,* 2010; Kane & Pontén, 2012).

Channel-cuts and their fills are commonly time transgressive (e.g. McHargue *et al.,* 2011; Sylvester *et al.,* 2011; Hubbard *et al.,* 2014; Hodgson *et al.,* 2016), formed by numerous energetic flows that excavated the channel. The preserved expression of flows that bypassed sediment further down-dip is composite erosion surfaces and associated heterogeneous channel-base-deposits. In the current study the term channel-base-deposit is used instead of the commonly used channel-base-drape (e.g. Barton *et al.,* 2010) because a drape infers low-energy or background depositional processes, whereas channel base facies commonly indicate repeated cycles of erosion, entrainment and deposition by high-energy flows (e.g. Mutti & Normark, 1987). The nature of channel-base-deposits is commonly used to infer the characteristics of their parent flows, and can be useful in predicting the presence or absence of sandstone down-dip (Walker, 1975; Mutti & Normark, 1987; Barton *et al.,* 2010; Hubbard *et al.,* 2014; Stevenson *et al.,* 2015; Li *et al.,* 2016).

This study documents an exhumed Permian slope channel complex set (Unit 5, Skoorsteenberg Formation) that crops out in the Tanqua depocentre, Karoo Basin, South Africa (Fig. 1A and B). A series of depositional strike, depositional dip, and oblique oriented cliff-faces permit documentation of the lateral, longitudinal, and vertical architecture of channel-fills in a mud-rich, fine-grained system (Fig. 1C). The objectives of this study are: (i) to elucidate the stratigraphic evolution of the channel complex set; (ii) to investigate the down-dip and across-strike architectural and facies variability within the channel complex set; (iii) to document the facies and distribution of channel-base-deposits; and (iv) to discuss the implications for reservoir connectivity and interpretation of subsurface data.

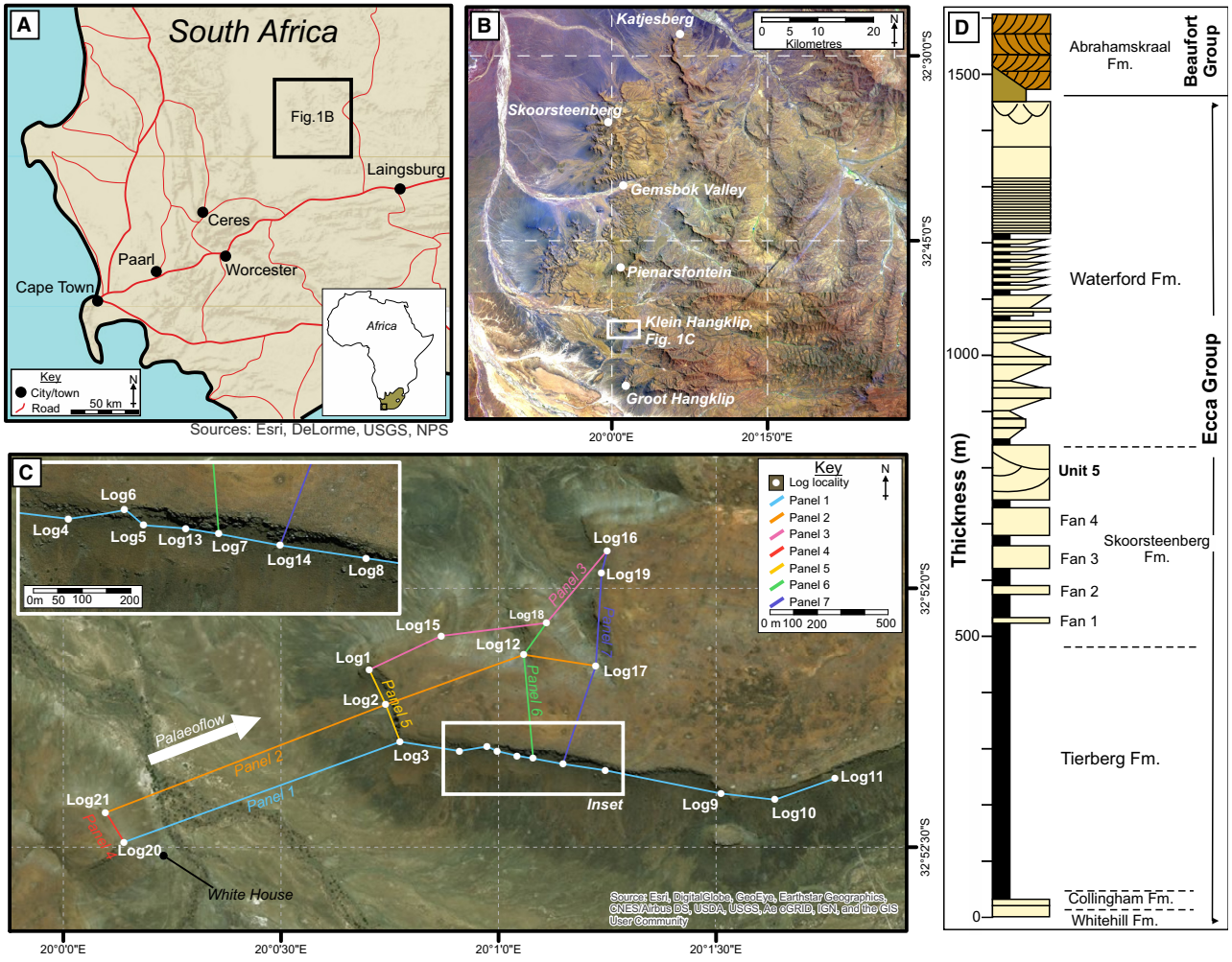

Fig. 1. Locality maps and stratigraphic context of the study area. (A) Location of the Tanqua depocentre, Karoo Basin (black box) in South Africa. (B) Location of the Klein Hangklip outcrop (white box) within the Tanqua depocentre, Karoo Basin. (C) Positions of logged sections and stratigraphic panels at the Klein Hangklip outcrop. (D) Summarised stratigraphic column of the Tanqua succession (modified from Wild *et al.,* 2005).

GEOLOGICAL SETTING

The Karoo Basin developed during the Permian due to subsidence induced by mantle flow processes associated with subduction of the Palaeo-Pacific plate, before transitioning to a retro-arc foreland basin related to an adjacent fold and thrust belt, from approximately 250 Ma (Cape Fold Belt; De Wit & Ransome, 1992; Veevers *et al.,* 1994; Visser & Praekelt, 1996; Viglietti *et al.,* 2017). The deposits of the Karoo Supergroup, comprising the glacial Dwyka Group, the marine Ecca Group and the non-marine Beaufort Group, record basin deepening followed by shallowing through the late Carboniferous to the Triassic (Fig. 1D; Smith, 1990; Bouma & Wickens, 1991; Wickens, 1994; Johnson *et al.*, 1996; Hodgson *et al.*, 2006). This study concerns the Ecca Group, which records a progradational, shallowing-upward marine succession (Fig. 1D; Smith, 1990; Bouma & Wickens, 1994; Hodgson *et al.,* 2006).

The Ecca Group in the Tanqua depocentre, located in the south-west of the Karoo Basin (Fig. 1), is subdivided into the Lower and Upper Ecca Group: The Lower Ecca Group consists of the relatively sand-starved basin-floor Prince Albert and Whitehill formations (Visser, 1994; Boulesteix *et al.*, 2019); the Upper Ecca Group includes the sand-starved basin-floor Tierberg Formation (Visser, 1994; Boulesteix *et al.*, 2019), the basin-floor to base of slope Skoorsteenberg Formation and slope to shallow-marine

Waterford Formation (Fig. 1D; Bouma & Wickens, 1991; Bouma & Wickens, 1994; Johnson *et al.,* 2001; Wild *et al.,* 2005; Hodgson *et al.,* 2006; Wild *et al.,* 2009; Poyatos-Moré *et al.,* 2016).

The Skoorsteenberg Formation is 450 m thick in the Tanqua Depocentre and comprises five sandstone-prone units. The lower four units are interpreted as a progradational succession of submarine fans (Fans 1 to 4), overlain by a fifth unit (Unit 5) interpreted as a base of slope to lower-slope system (Bouma & Wickens, 1991, 1994; Johnson *et al.*, 2001; Wild *et al.*, 2005; Hodgson *et al.*, 2006; Prélat *et al.*, 2009; Hansen *et al.*, 2019). Each fan is interpreted as a low-stand systems tract and is overlain by regionally correlated fine-grained packages interpreted as the combined transgressive and highstand systems tracts (Goldhammer *et al.,* 2000; Johnson *et al.,* 2001; Flint *et al.*, 2011).

This study focusses on Unit 5 in the Klein Hangklip study area located in the south of the Tanqua depocentre (Fig. 1B and C). Here, the preserved stratigraphy is 55 m thick, although Unit 5 is *ca* 100 m thick regionally. Unit 5 at Klein Hangklip is interpreted to represent a submarine slope environment consisting of intra-slope lobes, channel-fills and lateral channel splay deposits (Wild *et al.,* 2005). The channel-fills have an internal hierarchy and are interpreted as a series of channel complexes (Wild *et al.,* 2005). A regional fine-grained unit separates Unit 5 from the underlying Fan 4, which is subdivided into sandstone-rich Upper and Lower Fan 4 (Hodgson *et al.,* 2006; Spychala *et al.,* 2017; Hansen *et al.,* 2019).

METHODOLOGY AND DATA SET

This study utilises 21 sedimentary logs measured at 1 : 20 scale (Fig. 2). Logs were used to construct seven correlation panels; three oriented down depositional-dip and four oriented along depositional-strike (Figs 1C and 2). Correlations were made in the field by mapping key packages and surfaces. In addition, aerial and unmanned aerial vehicle (UAV) photographs were used to further support correlations in areas difficult to access and were used to guide and supplement geometric interpretations observed in the field. Data collected include lithology, bed thickness and palaeocurrents (n = 107) measured from ripple cross-lamination, wood-fragment long-axis orientation and channel incision surfaces.

FACIES AND CHANNEL HIERARCHY

The outcrops at Klein Hangklip have been interpreted as submarine channel-fills containing turbidites (Wild *et al.,* 2005). Six lithofacies were identified and are summarised in Table 1. The lithofacies are grouped into a channel-fill facies association.

Lithofacies description and interpretation

F1: Siltstone

Description. Fine-grained to coarse-grained siltstones form packages or caps to individual beds (Fig. 3A). Fine-grained siltstone packages appear homogenous at outcrop, though on a micro-scale siltstones in the Tanqua depocentre typically consist of 0.1 to 1.0 mm scale beds (Boulesteix *et al.*, 2019). Typically, coarse-grained siltstones are well-bedded (Fig. 3A), have bed thicknesses of 0.01 to 0.07 m, and are frequently rippled. Claystones were not observed in the study area.

Interpretation. Laminated siltstones which cap individual sandstone beds are interpreted to be deposited from the relatively dilute tail of turbidity currents (Bouma 1962; Walker, 1966a; Mutti & Ricci Lucchi, 1978; Stow & Bowen, 1980). Thick packages of 'laminated' siltstones are likely to have been deposited by numerous discrete and dilute turbidity currents (Piper, 1972; Morris *et al.*, 2014; Newport *et al.*, 2017; Boulesteix *et al.*, 2019). Rippled deposits are interpreted to form due to deposition and reworking by dilute, fully turbulent flows (e.g. Walker, 1965; Allen, 1982; Baas, 1994).

F2: Laminated sandstone

Description. Very fine-grained to fine-grained sandstone beds 0.05 to 2.5 m thick with alternating finer and coarser 0.5 to 1.0 mm thick laminae which are bed-parallel to sub-horizontal (Fig. 3B). Beds are commonly sharp-topped or amalgamated, but rare examples grade to siltstone. Commonly, laminated sandstones form an upper division to a sandstone bed, which has a lower, structureless sandstone division. Organic material, including leaf or wood-fragments, is commonly preserved parallel to laminae.

Interpretation. Sandstones with parallel lamination can be deposited from the repeated formation and collapse of near-bed layers termed 'traction carpets' in high-concentration flows (Dzulynski & Sanders, 1962; Hiscott & Middleton, 1979; Lowe, 1982; Sohn, 1997; Sumner *et al.*, 2008); or by the

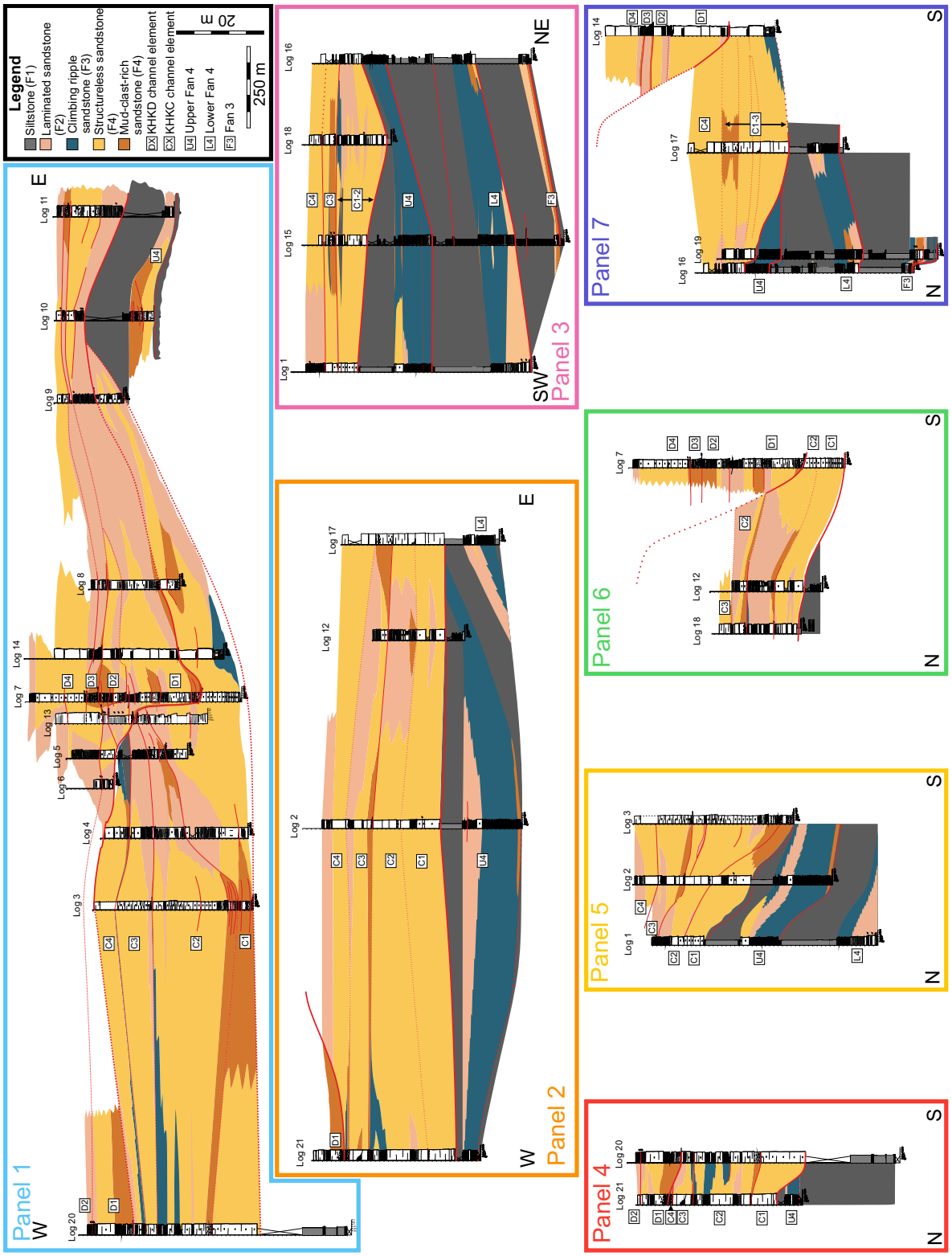

Fig. 2. Sedimentary logs and correlation panels from the study area. Solid red lines are constrained erosion surfaces, dashed red lines represent inferred correlation of surfaces. Refer to Fig. 1C for locations.

Table 1. Lithofacies observed in the field area.

Code	Lithofacies	Unit thickness (m)	Grain-size	Description	Interpretation
F1	Siltstone	0.01–14.0	Fine to coarse-grained siltstone	Fine-grained siltstones, with interbedded coarse-grained siltstone packages. Fine-grained siltstone packages appear structureless, while coarser-grained siltstone packages are well-bedded, and often ripple cross-laminated	Deposition from dilute low-density turbidity currents, or the tails of bypassing turbidity currents (Mutti, 1977; Newport *et al.,* 2017; Boulesteix *et al.,* 2019)
F2	Laminated sandstone	0.05–2.5	Very fine-grained sandstone	Alternating 0.1 to 1.0 mm scale coarser and finer laminae. Plant fragments and organic debris are locally present parallel to laminae. Typically, beds have sharp tops and bases which can be amalgamated, or can grade to siltstone	Layer by layer deposition from repeated development and collapse of near-bed traction carpets (Sumner *et al.,* 2008) and migration of low-amplitude bed-waves (Best & Bridge, 1992; Sumner *et al.,* 2008)
F3	Rippled sandstone	0.1–2.1	Very fine-grained sandstone	Present as either individual beds or as part of packages that reach up to 7 m thick. Typically consists of ripples with supercritical angles of climb interbedded with planar laminated sandstone and infrequent climbing ripples with subcritical angles of climb. The lower division of the bed typically consists of laminated sandstone	Deposition from long-lived, surging flows with high rates of sediment fallout (Allen, 1991; Baas *et al.*, 2000; Kane & Hodgson, 2011; Jobe *et al.*, 2012; Morris *et al.*, 2014)
F4a F4b	Structureless sandstone	0.02–10.0	Very fine to lower fine-grained sandstone	Typically, structureless and ungraded to weakly normally-graded; F4a are well-bedded and typically <1 m thick; F4b are thick amalgamated packages with poorly-defined bedding that form packages up to 10 m thick. Commonly show evidence of dewatering, though typically more evident in F4b. Mudstone chips may be present locally	Rapid settling from a high concentration flow (e.g. Lowe, 1982)
F5a F5b	Cross-bedded sandstone	0.3–1.0	Lower fine-grained sandstone	Cross-bedded sandstones with foresets that are tens of centimetres high. Foresets can be clast rich, or clast poor	Deposition and reworking from fast-moving, long-lived, low-concentration turbidity currents (Allen, 1970a, 1982; Baas *et al.*, 2004; Sumner *et al.*, 2012; Talling *et al.*, 2012)

Table 1. (continued)

Code	Lithofacies	Unit thickness (m)	Grain-size	Description	Interpretation
F6	Mud clast-rich structureless sandstone	0.05–6.0	Very fine to lower fine-grained sandstone	These can be present as either individual beds or can form packages up to 6 m thick. Typically consists of ungraded sandstone containing abundant millimetre-scale to centimetre-scale mudstone clasts, which are distributed throughout or aligned in discrete horizons within the bed	Deposition from high-concentration turbidity currents which were erosive either locally or up depositional dip
F7	Argillaceous sandstone	0.1–1.0	Very fine to lower fine-grained sandstone	Poorly sorted and clay-rich sandstone, frequently mudstone-clast-rich throughout the bed. Commonly scoured. Observed as composite packages in channel-base-deposits	Deposition from highly concentrated, erosive flows transitional between turbulent and laminar flow regimes due to clast entrainment and breakup (Haughton *et al.*, 2003; Baas *et al.*, 2009; Kane & Pontén, 2012; Pierce *et al.*, 2018)

migration of low-amplitude bed-waves in low-concentration flows (Southard, 1991; Best & Bridge, 1992). It is challenging to distinguish which depositional process forms a given parallel laminated deposit at outcrop (e.g. Talling *et al.*, 2012). However, parallel laminated sandstones at Klein Hangklip are frequently associated with thinner-bedded deposits in channel off-axis and margin positions, where turbidity currents were likely relatively low-concentration (Altinakar *et al.*, 1996; Hansen *et al.*, 2015; Jobe *et al.*, 2017), and therefore migration of low-amplitude bed-waves is preferred.

F3: Rippled sandstone

Description. Very fine-grained sandstone beds with well-developed current-ripple cross-lamination (Fig. 3C). Typically, ripple laminations develop as divisions within a bed overlying laminated or structureless sandstone (Fig. 3C). Divisions are 0.05 to 0.8 m thick, and form packages up to 2.1 zm thick. Ripple laminations commonly exhibit supercritical angles of climb with stoss-side preservation (Fig. 3C). Less frequently, ripple laminations have subcritical angles of climb, and are associated with thinner divisions (<0.1 m) and reworked bed tops.

Interpretation. Ripple laminated sandstones are deposited from fully turbulent flows, or parts of flows, which are low concentration, have relatively low rates of fallout, and can rework the bed (e.g. Walker, 1965; Allen, 1982; Southard, 1991; Baas, 1994, 1999). Thick packages of rippled sandstone with supercritical angles of climb are interpreted to be deposited by sustained, relatively dilute, flows in which the depositional rate was in excess of that of bedform migration (e.g. Sorby, 1908; Allen, 1970b, 1991; Baas *et al.*, 2000; Jobe *et al.*, 2012).

F4: Structureless sandstone

Description. Very fine-grained to fine-grained sandstone beds 0.02 to 6.7 m thick, which form packages up to 10 m thick. Beds are apparently structureless and ungraded to weakly graded (Fig. 3D and E). Sandstone beds are frequently dewatered, which is typical of sandstones in the basin (e.g. Hodgson *et al.*, 2006). Beds often form either: (i) highly amalgamated packages in which bedding surfaces are challenging to distinguish (Facies F4b; Table 1; Fig. 3E); or (ii) relatively thinner-bedded sandstones in which bedding surfaces are distinguishable, even if amalgamated (Facies F4a; Table 1; Fig. 3D). Plant fragments can be

observed along bed tops, or rarely observed within the bed itself. Mudstone clasts are commonly observed on bed tops, or isolated within the bed.

Interpretation. Apparently structureless sandstones are deposited incrementally from high-concentration, near-bed, parts of flows in which high depositional rates inhibit the development of tractional bedforms (Kuenen, 1966; Lowe, 1982; Kneller & Branney, 1995; Baas *et al.*, 2004; Leclair & Arnott, 2005; Sumner *et al.*, 2008). Rapid near-bed aggradation is interpreted to create excess pore pressures, resulting in dewatering (Lowe, 1975). An alternative mode of deposition of is from the *en masse* freezing of sandy debris flows (e.g. Shanmugam, 1996). However, structureless sandstones in the field area commonly grade laterally into laminated sandstones and do not pinch-out abruptly, which are suggestive of spatial changes in flow behaviour, as opposed to freezing of the flow (Talling *et al.*, 2012, 2013). As such, sandstones here are interpreted as the product of high-concentration near-bed layers of turbidity currents.

F5: Cross-bedded sandstone

Description. Very fine-grained to fine-grained cross-bedded sandstones with foresets that reach tens of centimetres in height are rarely observed in the study area (Fig. 3F). Foresets may contain abundant mudstone-clasts aligned parallel to laminae, though more typically clasts are absent.

Interpretation. The development of dune-scale cross-bedded sands is suppressed at high near-bed concentrations and sediment fallout rates (Lowe, 1988; Baas *et al.*, 2011). Dune-scale

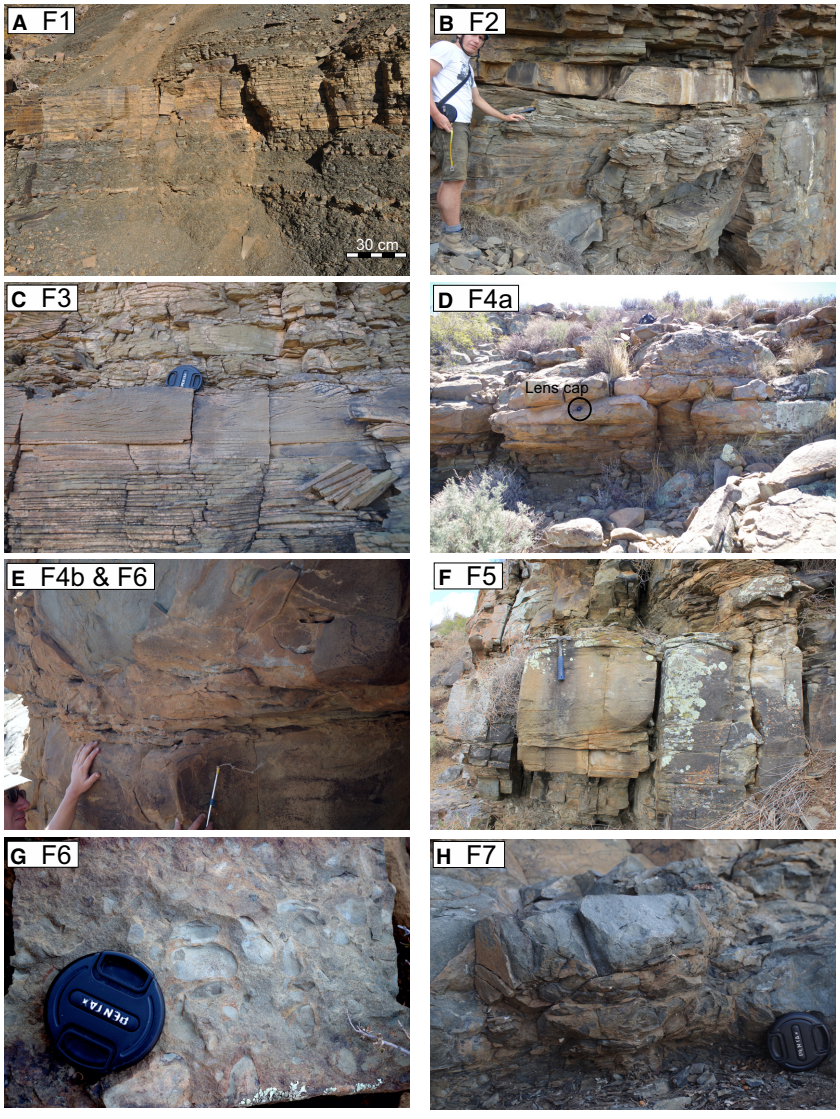

Fig. 3. Representative photographs of lithofacies in the study area. (A) Bedded siltstone (F1). (B) Laminated sandstone (F2). Person for scale is *ca* 1.8 m tall. (C) Rippled sandstone (F3). Lens cap for scale, 60 mm diameter. (D) Medium-bedded amalgamated sandstone (F4a). (E) Thick-bedded amalgamated sandstone (F4b) with a mudstone-clast-rich base (F6). (F) Cross-bedded sandstone (F5b). Hammer for scale, 27 cm long. (G) Mudstone-clasts concentrated on an erosion surface (F6). (H) Argillaceous sandstone (F7) within a channel-base-deposit.

cross-bedding in deep-water systems is therefore interpreted to form from long-lived, fast-moving, relatively dilute flows that had low rates of sediment fallout (Walker, 1965; Allen, 1970a; Sumner *et al.*, 2012).

F6: Mud-clast-rich sandstone

Description. Mudstone-clast-rich sandstones are structureless. They also contain an abundance of mudstone clasts distributed throughout the bed or package (Fig. 3E and G).

Interpretation. Mudstone-clast-rich sandstones are interpreted to be deposited from near-bed parts of high-concentration flows in which turbulence was suppressed (e.g. Lowe, 1982). Mudstone clasts are likely sourced from either erosion and entrainment of local substrate (Walker, 1966a; Johansson & Stow, 1995; Butler & Tavarnelli, 2006; Southern *et al.*, 2015) or transported in the flow from further updip (Johansson & Stow, 1995; Hodgson, 2009).

F7: Argillaceous sandstone

Description. Argillaceous, very fine-grained to fine-grained sandstones are observed only in axial channel-base-deposits (Fig. 3H). Typically, beds are 0.1 to 0.4 m thick, and locally form composite packages up to 1 m thick, are relatively poorly sorted, darker in colour and are more fissile than other sandstones. Argillaceous sandstones are usually mudstone-clast-rich, with clasts in varying stages of break-up (Fig. 3H).

Interpretation. Poorly sorted, argillaceous sandstones with an elevated matrix content are interpreted to be deposited under flows transitional between turbulent and laminar (e.g. Wang & Larsen, 1994; Baas & Best, 2002; Sylvester & Lowe, 2004; Baas *et al.*, 2009; Kane & Pontén, 2012; Kane *et al.*, 2017). The common occurrence of argillaceous sandstones overlying erosion surfaces suggests that the source of flow transformation was likely local substrate entrainment (Southern *et al.*, 2015; Fonnesu *et al.*, 2016), which suppressed turbulence, as opposed to longitudinal flow transformation (e.g. Haughton *et al.*, 2009; Hodgson, 2009; Kane *et al.*, 2017).

Facies associations

One major facies association is identified in the study area. This is a channel-fill facies association, which is described below.

FA1: Channel-fill

Channel-fills can exhibit a wide-range of fill-styles, which can be partially preserved, symmetrical or asymmetrical; and can be filled with different proportions of sandstone, mudstone or debrites. Such variability can occur at the individual channel element, complex, and complex set scale (e.g. Pickering & Corregidor, 2005; Mayall *et al.*, 2006; Pyles *et al.*, 2010; Moody *et al.*, 2012; Bayliss & Pickering, 2015; Zhang *et al.*, 2015; Li *et al.*, 2016). Despite this, a generalised facies association for the Klein Hangklip channel-fill is proposed. Divergence from these descriptions across different channel elements, complexes and the channel complex set are described in the results.

Where symmetrical, a given channel-fill typically exhibits a gull-wing-like geometry. The channel axis is located at the thickest point of the channel-fill, and predominantly consists of comparatively thick-bedded, amalgamated F4a, F4b and F6 (Table 1; Figs 3 to 5). Channel off-axis positions overlie the steep erosional cut of the channel, with the fill being stratigraphically thinner, and comprise comparatively thinner-bedded F4, F4b and F2; with subordinate F6 (Figs 3 to 5). Channel margin positions overlie the low-gradient, upper parts of the channel-cut, corresponding to the upper and outer parts of a gull-wing geometry. Channel margin deposits are comparatively thin and are laterally extensive (Fig. 4). Channel margin facies typically consist of comparatively thin-bedded F2 and F4a, with localised F1 and F3 (Figs 3 to 5).

Channel hierarchy

Submarine slope channel-fills are hierarchically organised (Fig. 5; e.g. Sprague *et al.*, 2002, 2005; Di Celma *et al.*, 2011; McHargue *et al.*, 2011; Moody *et al.*, 2012; Macauley & Hubbard, 2013; Stright *et al.*, 2014; Li *et al.*, 2016). The hierarchy used in the current study is based on Sprague *et al.* (2002, 2005), though note the substitution of 'channel fill' for 'channel element'; from the smallest to the largest scale, the hierarchy consists of: (i) beds/facies that share similar lithologies; (ii) storeys, which consist of beds filling an individual erosion surface or scour (Friend *et al.*, 1979); (iii) channel elements, which represent a single cycle of cut-and-fill (Fig. 5), and can contain numerous storeys; (iv) channel complexes formed from two or more nested channel elements (Fig. 5); and (v) channel complex sets formed by two or more

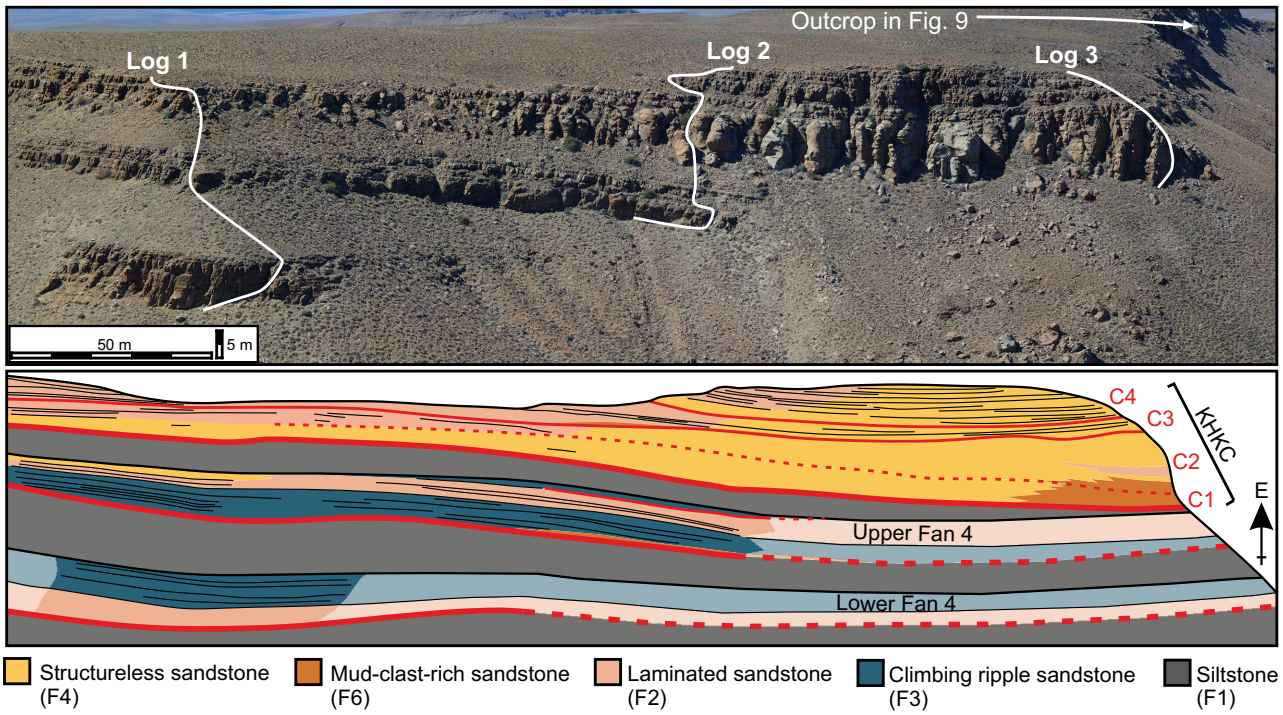

Fig. 4. Photopanel interpretation of an across-depositional-strike oriented cliff-face. The channel-fill incises from the channel margin in the north to the channel axis in the south, where it may incise the top of Upper Fan 4. The channel axis (for example, Log 3) is thicker and contains thick-bedded F6 and F4b in lower channel elements, and bedded F4a in upper channel elements. The off-axis (for example, Log 2) is thinner and comprises bedded F4b in lower channel elements, and bedded F4a and F2 in upper channel elements. Channel margin positions (for example, Log 1) comprise bedded F4a in lower channel elements, and bedded F2 in upper channel elements.

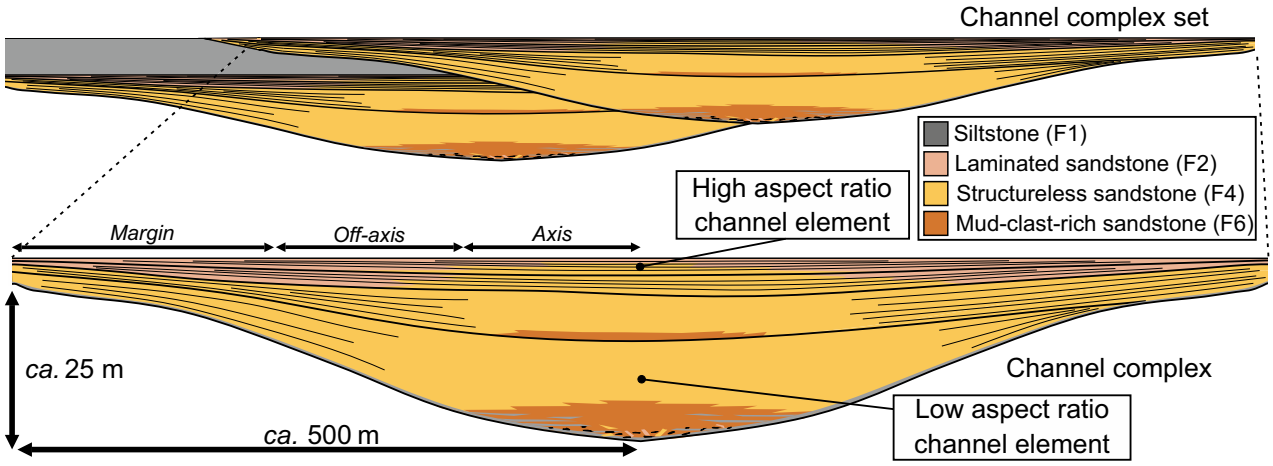

Fig. 5. Schematic summary of the hierarchical scheme applied to the Klein Hangklip channel-fill. 'Channel complex set' is the largest hierarchical level observed and consists of two channel complexes, each comprising four channel elements. Sub-environment geometries and facies distributions are schematically illustrated based on previous work (Mutti, 1977; Campion *et al.*, 2000; Sullivan *et al.*, 2000; Eschard *et al.*, 2003; Beaubouef, 2004; Macauley & Hubbard, 2013).

stacked channel complexes (Fig. 5). This hierarchical scheme has been applied to the Unit 5 succession based on scale and stacking patterns; and by correlation of logs and mapping of bounding surfaces both in the field and using aerial photography.

RESULTS

Architectural element descriptions

The architectural elements that make up the Klein Hangklip channel complex set are described below. The channel complex set is interpreted to consist of two channel complexes: stratigraphically, 'KHKC' and 'KHKD', each of which is made up of four channel elements.

Channel element 1: KHKC

The exposed outcrop of KHKC has a lenticular geometry (Fig. 4), representing approximately one half of the original channel complex from its left-hand channel margin to the channel-axis (relative to palaeoflow; Fig. 6). KHKC incises into the underlying siltstones and locally incises Upper Fan 4 (Fig. 6). The maximum observed incision is 20.5 m. The base of KHKC is rarely exposed, though the channel-base-deposit is observed 100 m to the south of Log 19 where KHKC incises F3 facies of Upper Fan 4 (Fig. 7A). KHKC is at least 890 m wide, has a maximum thickness of 32.9 m at Log 3 (Fig. 2; Panel 5), and thins and fines northward (Fig. 6; Panels 5 to 7). The minimum thickness of KHKC is 9.5 m at the channel margin position of Log 16 (Fig. 2; Panel 7), although KHKC visibly continues to thin for 125 m to the north of that position. No external levées belonging to KHKC are identified, although their existence cannot be ruled out. If levées are present, they are likely to be siltstone-prone, and weather recessively, resulting in exposures being covered by vegetation and scree. Four channel elements are identified in KHKC; these are (KHK) C1 to (KHK) C4.

KHKC1: C1 is lenticular in geometry with a maximum thickness of 10.2 m at its axis (Log 20), and is 5.4 m thick in the channel margin at Log 18 (Figs 4 and 6). C1 continues to thin northward; however, it becomes increasingly challenging to discern individual channel elements. The base of C1 is rarely exposed, except south of Log 19 (Figs 1C and 7A), where it comprises: (i) a basal incision surface lined by mudstone clasts which cuts into underlying sandstones; overlain by (ii) 0.2 m of thin-bedded coarse siltstone; and (iii) 1.1 m of lenticular thin-bedded sandstones, with rare localised mudstone clasts and medium-bedded sandstones that lie on a subtle erosion surface into thin-bedded sandstones (Fig. 7B). The upper surface of the channel-base-deposit is mudstone-clast-rich and is immediately overlain by KHKC1. The channel-base-deposit is poorly exposed at Log 3, where a 0.1 m thick (minimum) mudstone-clast-rich siltstone lag is observed below the basal F4 of the channel-fill. The channel axis (for example, Log 3; Fig. 2) of C1 is composed of amalgamated F6 with mudstone-clast-rich bed tops at the base, overlain by F4b (Fig. 4). F6 beds decrease in number and mudstone clasts reduce in size stratigraphically upward (Figs 4 and 6). The channel margin of C1 primarily comprises F4a, although F2 and F3 are observed locally (Figs 4 and 6).

KHKC2: C2 is 16.8 m thick at its channel axis at (Log 3; Fig. 2; Panel 4), thinning to 6.2 m to the north-east at Log 18, and 3.5 m to the south at Log 13 (Fig. 8). The base of C2 incises into C1 and is marked by a channel-base-deposit that has variable facies. In the westernmost logged sections (Logs 20 and 21), the channel-base-deposit of C2 is a basal mudstone-clast-rich layer overlain by a 0.1 to 0.2 m thick fine siltstone with localised mudstone clasts. One kilometre down-dip to the east (Log 3) the base of C2 is characterised by amalgamated, mudstone-clast-rich sandstones that are locally eroded through a thin siltstone bed (Fig. 8). At Logs 4, 5 and 13, the channel-base-deposit of C2 is expressed as a clast-rich composite channel-base-deposit that is up to 1.5 m thick with multiple composite scour surfaces. The channel-base-deposit is composed of siltstone with decimetre-scale rounded and angular sandstone clasts, remobilised bedded sandstones up to up to 1 m in length, and abundant mudstone clasts that range from centimetres to a metre in length. The deposit is also locally expressed as a 0.3 m thick clast-rich siltstone with thin beds of discontinuous clay-rich sandstones, or as an amalgamation surface with the underlying sandstones of C1, mantled by mudstone clasts. The fill of C2 varies spatially, both laterally from channel axis to channel margin positions, and in different panels down depositional dip (Figs 6 and 8). Typically, the channel axis comprises F4b, with F6 locally observed in the lower 2 m (Figs 6 and 8). Up to 4.5 m of F3 is observed in the channel axis of Logs 20 and 21 (Fig. 6; Panel 4). Bedding becomes less ambiguous as amalgamation decreases towards off-axis and channel margin positions (Fig. 4); this is accompanied by a decrease in bed thickness, and an increase in the proportion of F4a and F2 (Figs 4 and 6).

KHKC3: The basal erosion surface and channel-base-deposit of C3 are relatively flat-lying and

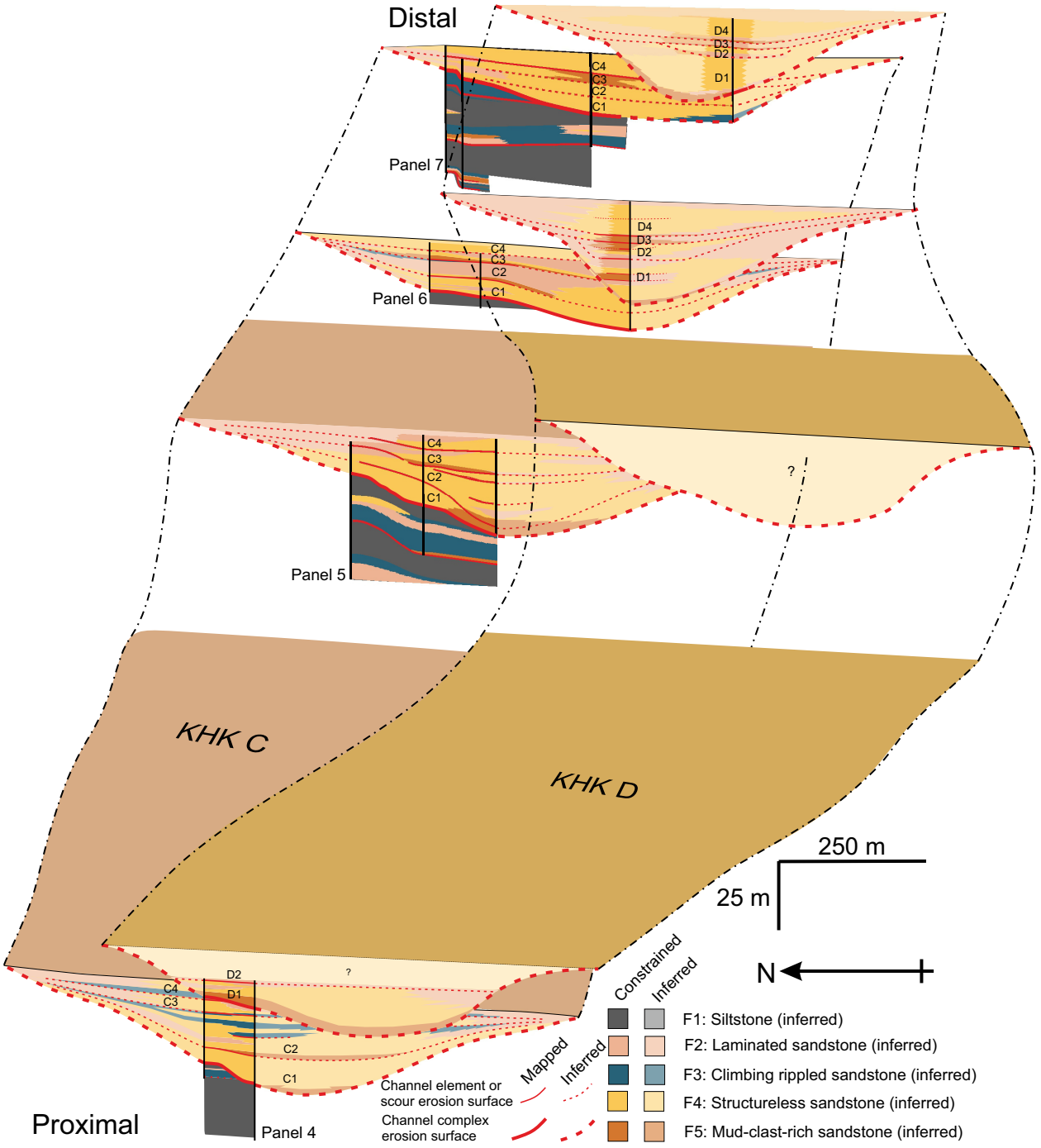

Fig. 6. Depositional strike-oriented correlation panels. Panels are arranged from proximal (bottom) to distal (top) to illustrate changes in facies and geometries.

have been identified at outcrop through an abrupt stratigraphic change in facies from thick-bedded to relatively thin-bedded sandstones (Fig. 4). C3 has a tabular geometry relative to those observed in C1 and C2 (Figs 4 and 6). The fill of C3 has a maximum thickness of 8 m at Log 3, which is located in the axis of KHKC (Figs 2 and 4), but is typically 3 to 4 m thick elsewhere (Fig. 2). The channel-base-deposit of C3 is laterally variable, comprising a 5 to 20 cm siltstone at Logs 4, 5, 16, 18 and 20 (Fig. 2), a clast-rich siltstone at Logs 1, 2 and 21 (Fig. 2), and amalgamated thin beds at Logs 3, 12 and 15 (Fig. 2). The fill of C3 predominantly consists of

F4a and F4b (for example, Log 3; Table 1; Figs 4 and 6). Channel axis and off-axis positions contain F6, which is typically located near the base of the channel element (Figs 4 and 6). Bed thickness and degree of amalgamation decrease into channel margin positions, which comprise F2 and F4a, with rare F6 overlying the channel-base-deposit (Figs 4 and 6). In southern channel margin localities (Logs 4 and 5) the fill of C3 is dominated by F2, with localised F4a (Figs 8 and 9).

KHKC4: C4 is the uppermost channel element of the KHKC channel complex and has a relatively tabular geometry (Figs 6 and 8). The total thickness of C4 is unknown as the upper portion is poorly-exposed and therefore thicknesses should be considered a minimum value. C4 is thickest in the channel axis at Log 17 (7.8 m; Fig. 2), the measured thicknesses at other localities are typically 3 to 5 m (Figs 6 and 8). The C4 erosion surface and channel-base-deposit are rarely exposed, and they have a variable character where they can be observed. The channel-base-deposit is typically a thin siltstone (<10 cm, locally up to 30 cm; Fig. 7E) that may contain mudstone clasts, although the base is also locally expressed as an amalgamation surface. The facies of the C4 channel element fill is variable, particularly from channel axis to channel margin. In axial positions, C4 comprises F4a with local F4b and F6 (Figs 4 and 6). Off-axis positions consist of F2 and F4a, with F4b and F6 locally present down-dip (Figs 6 and 8). Channel margin positions are predominantly composed of F2, with localised F4a (Figs 4 and 6). The south-eastern most position of C4, Log 5, has 2 m of F1 at the base and is overlain by 1 m of F3 (Fig. 9).

Channel element 2: KHKD

The uppermost sandstones of KHKC are overlain by approximately 2 m (minimum) of siltstone at Log 5, which is incised by the erosion surface of the overlying channel-fill, KHKD. The KHKD channel complex is exposed in a 2.7 km wide (minimum) outcrop oriented oblique to strike, (Panel 1; Figs 2 and 9) and is not exposed on the north face of Klein Hangklip. KHKD is thickest (39.0 m) at Log 7 (Fig. 6) and thins into the east and west channel margins to 6.2 m (Log 10) and 4.5 m thick (Log 6), respectively (Figs 2 and 8). The western composite-cut of KHKD is steeper than the eastern channel-cut (Figs 8 and 9). The margin of the channel complex pinches out approximately 40 m to the west of Log 6 (Figs 8 and 9). The pinchout of the eastern margin is not observed due to the oblique nature of the outcrop, although the thinning and change of facies to predominantly laminated sandstone suggests that it is located south of Logs 9 and 10 (see Fig. 10). The channel axis of KHKD incises a maximum of approximately 22.5 m into the underlying fill of KHKC at Log 7 (Figs 8 and 9). Similar to KHKC, no external levées are identified, although they are possibly present but not exposed. Four channel elements have been identified in KHKD (D1 to D4):

KHKD1: D1 is the oldest channel element in the KHKD channel complex. D1 is mapped over 2.7 km in Panel 1 and is best exposed on the southern face of the outcrop (Figs 8 and 9). The basal erosion surface and channel-base-deposit of KHKD1 form the base of the channel element and are well-exposed across the outcrop (Figs 9 and 11A). In channel margin positions, the channel-base-deposit is predominantly composed of at least 11 cm of F1 with rare mudstone clasts and lenticular very fine sandstone beds. In channel off-axis positions, the channel-base-deposit is 5 to 30 cm thick and consists of F1 and thin F4a, which are discontinuous and locally slumped (Fig. 11B). In channel axis positions, the channel-base-deposit is composite, up to 2.5 m thick, and comprises: amalgamated F6; remobilised clasts that are commonly sheared [Fig. 11C; F1, which is commonly amalgamated; F7 (Fig. 11C); and F4b, which is locally amalgamated with underlying KHKC sandstones (Fig. 11D)].

KHKD1 is up to 17.0 m thick in the channel axis at Log 7 (Fig. 2) and thins laterally to 2.5 m and 2.2 m at its western and eastern channel margins at Logs 6 and 10, respectively (Panel 1; Figs 2 and 8). In proximal positions, D1 thins northward from 9.5 m at Log 20, to 6.3 m at Log 21 over 70 m (Fig. 6). The proportion of F4a decreases, which is accompanied by an increase in F2 (Fig. 6). On the southern outcrop face, the channel-base-deposit of D1 is 1.5 m thick and composite at Log 7 (Fig. 11C), becoming thinner and more silt-prone to both the east and west at Logs 9 and 6, respectively (Fig. 2; Panel 1). The facies distribution of D1 is asymmetrical (Figs 8 and 9). Towards the west (Logs 5 and 6; Fig. 2), D1 predominantly consists of F2 (Figs 8 and 9), with abundant laminae-parallel plant fragments. The proportion of F4b and amalgamated F6 increase into the thickest and most axial parts of

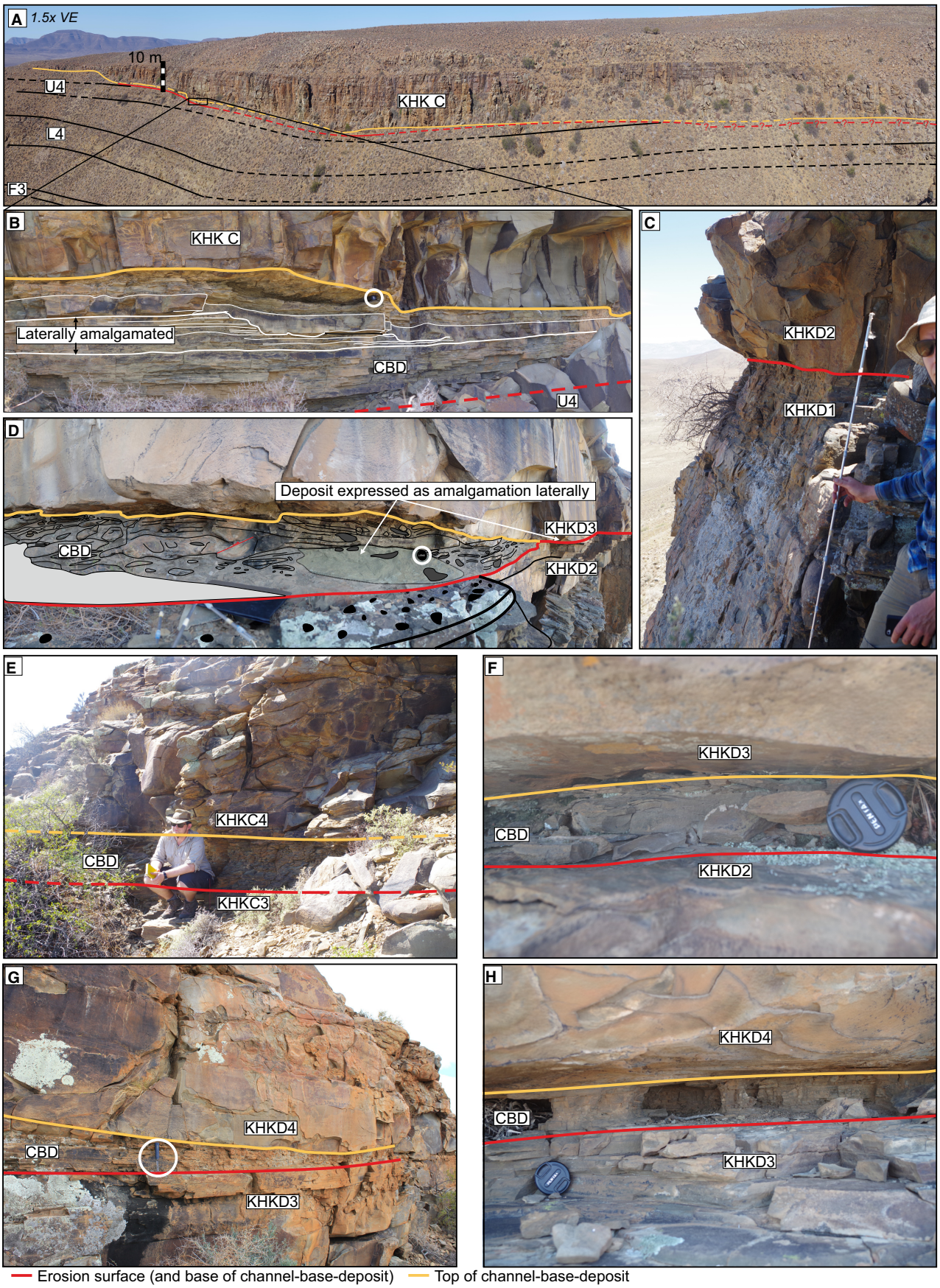

Fig. 7. Erosion surfaces and channel-base-deposits (CBDs). (A) KHKC incised into underlying stratigraphy near Log 19 on the north of Klein Hangklip. (B) Inset of (A), the basal deposit of C1 observed at a channel margin position. The deposit is 1.5 m thick and predominantly comprises thin-bedded sandstones deposited from dilute flows, and medium-bedded sandstones which incise into underlying beds, deposited from larger flows. Lens cap (60 mm diameter) circled for scale. (C) Sharp erosion surface between channel elements D1 and D2 which lacks a channel-base-deposit. Logging pole markings spaced every 10 cm. (D) Channel-base-deposit of D3 at its most composite, located on the outer bend of the channel-fill. The composite deposit is incised by overlying sandstone and laterally identified as a sandstone amalgamation surface. Lens cap circled. (E) A *ca* 30 cm thick siltstone-rich channel-base-deposit between channel element C3 and C4. (F) Typical non-composite character of the D3 channel-based-deposit observed at other localities. (G) Thin-bedded channel element scale channel-base-deposit between D3 and D4. Hammer circled (27 cm long). (H) Thin-bedded coarse siltstone channel-base-deposit between channel elements D3 and D4.

D1 at Logs 7 and 14, adjacent to the steep western channel-cut (Fig. 9). Thin (<10 cm) layers of F1 wedge out from the steep western channel-cut (Fig 11B). F1 beds are incised by overlying deposits that contain abundant clasts of F1 towards the axial positions (Fig. 11B and C). The eastern channel-cut, from Log 9 to Log 8, has a relatively shallower gradient (Fig. 8). The channel-fill exhibits a gradual decrease in F4b and F6 away from the channel axis, and a concurrent proportional increase in F2 to the east of Log 7 (Fig. 8). Stratigraphically within D1 the proportions of F4b and F6 decrease upward with a concurrent increase in F2 (Figs 8 and 9). Locally, F5 is observed at the base of D1 at Log 20 (Fig. 3F) and Log 8.

KHKD2: D2 has a subtle unconformable contact with D1 and can be traced on aerial photographs between Logs 13 and 14 (Fig. 9). D2 has a lenticular geometry, thickening from east of Log 13 towards Log 7 (Fig. 9), but is poorly exposed to the east where the cliffs are lichen-covered. The base of D2 is characterised by a sharp contact between thin-bedded F2 of D1, to thick-bedded F2 (Fig. 7D) and 1.2 m of F4b of D2, respectively. The upper-fill of D2 consists of 3.3 m of bedded (0.02 to 0.3 m thick) F6 and also contains localised 0.1 to 0.5 m thick scour-fills consisting of centimetre-scale beds of F4a and thin-bedded F6.

KHKD3: D3 has a relatively tabular geometry, with thicknesses between 3.9 m and 1.2 m (Fig. 9). The channel-base-deposit of D3 is 0.1 to 0.3 m thick, flat-lying, laterally continuous, and consists predominantly of F1, which is locally clast-rich. Localised amalgamation of thin-bedded F4a is also observed. However, adjacent to the steeper western channel cut of KHKD, the channel-base-deposit of D3 is expressed as an up to 0.3 m thick composite deposit consisting of mudstone-clasts and sandstone-clasts and argillaceous sandstones. Laterally to the east, over 2 to 3 m, this channel-base-deposit is preserved as a sandstone amalgamation surface. In all cases the channel-base-deposit overlies a sandstone bed mantled with mudstone clasts. At Logs 13 and 7, D3 consists of F4b and F6 (Figs 8 and 9). The proportions of F4b and F6 decrease to the east and west with a concurrent increase in the proportion of F2 (Figs 8 and 9).

KHKD4: D4 is the uppermost channel element identified in the KHKD channel complex. The thickness of D4 is variable, from 13.0 m at Log 7 to 1.4 m thick at Log 10 (Fig. 2); these are minimum recorded thicknesses due to modern erosion. The basal surface of D4 is relatively flat-lying, suggesting that the channel element has an overall tabular geometry (Figs 8 and 9). The channel-base-deposit of D4 is typically characterised by fine-grained, thin-bedded F4a, which incise into and amalgamate with the underlying sandstones of D3 (Fig. 7G and H). Locally, the channel-base-deposit comprises 10 cm of F1, which is clast-rich and overlain by centimetre-thick to decimetre-thick beds of F6. Where KHKD is thickest, the fill of D4 predominantly comprises F6b at the base, and localised F2 in the upper 2 to 3 m (Figs 8 and 9). Where KHKD thins to the east, D4 consists of F4a and F4b, with localised F2 (Figs 8 and 9). Conversely, to the west D4 predominantly comprises F2 at Log 5 (Figs 8 and 9).

Palaeocurrents

Unit 5 at Klein Hangklip is interpreted to have north-eastward oriented palaeoflow (Wild *et al.,* 2005). Palaeoflow directions of the Hangklip channel-fills are constrained by ripple cross-laminations, channel-cut orientations, outcrop constraints, and preferential orientation of wood-fragment long axes.

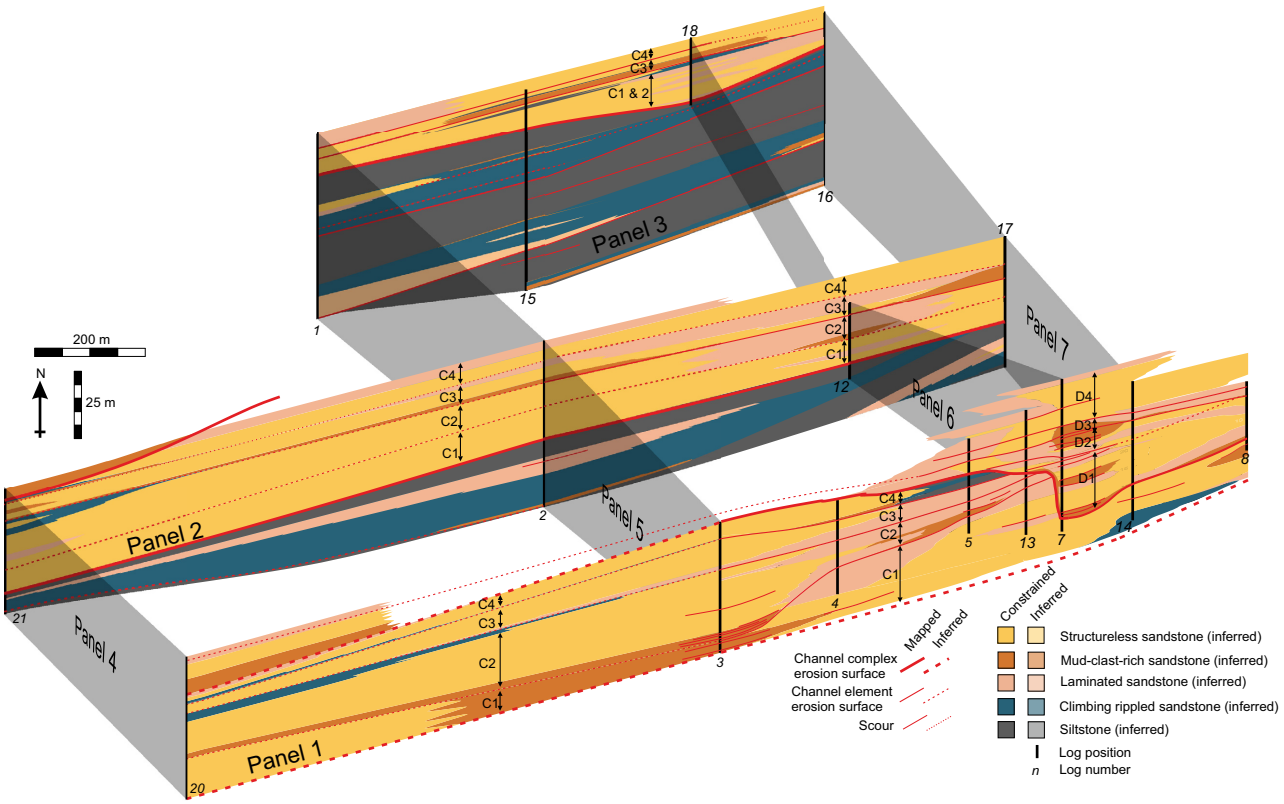

Fig. 8. Depositional dip-oriented panels from proximal (left) to distal (right). Facies are spatially variable, in both depositional dip-oriented and strike-oriented directions.

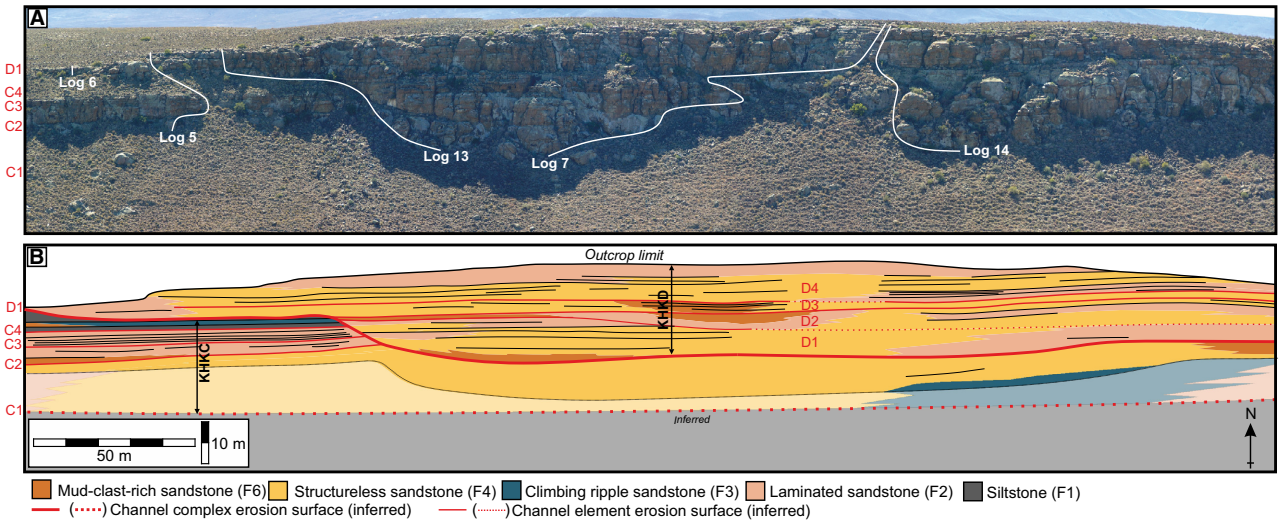

Fig. 9. (A) Photomosaic of an east–west oriented cliff face on the southern side of Klein Hangklip. (B) Annotated overlay showing architectural and facies relationships. KHKD incises into KHKC from west to east, cutting into channel margin facies of channel elements C2, C3 and C4. The channel axis of the KHKD channel complex comprises greater proportions of F4b and F6 compared to the channel off-axis and margin positions to the east and west. Facies distribution is asymmetrical, with sharper pinch-outs and facies transitions against the steeper western margin (outer bank) compared to the shallower eastern margin (inner bank).

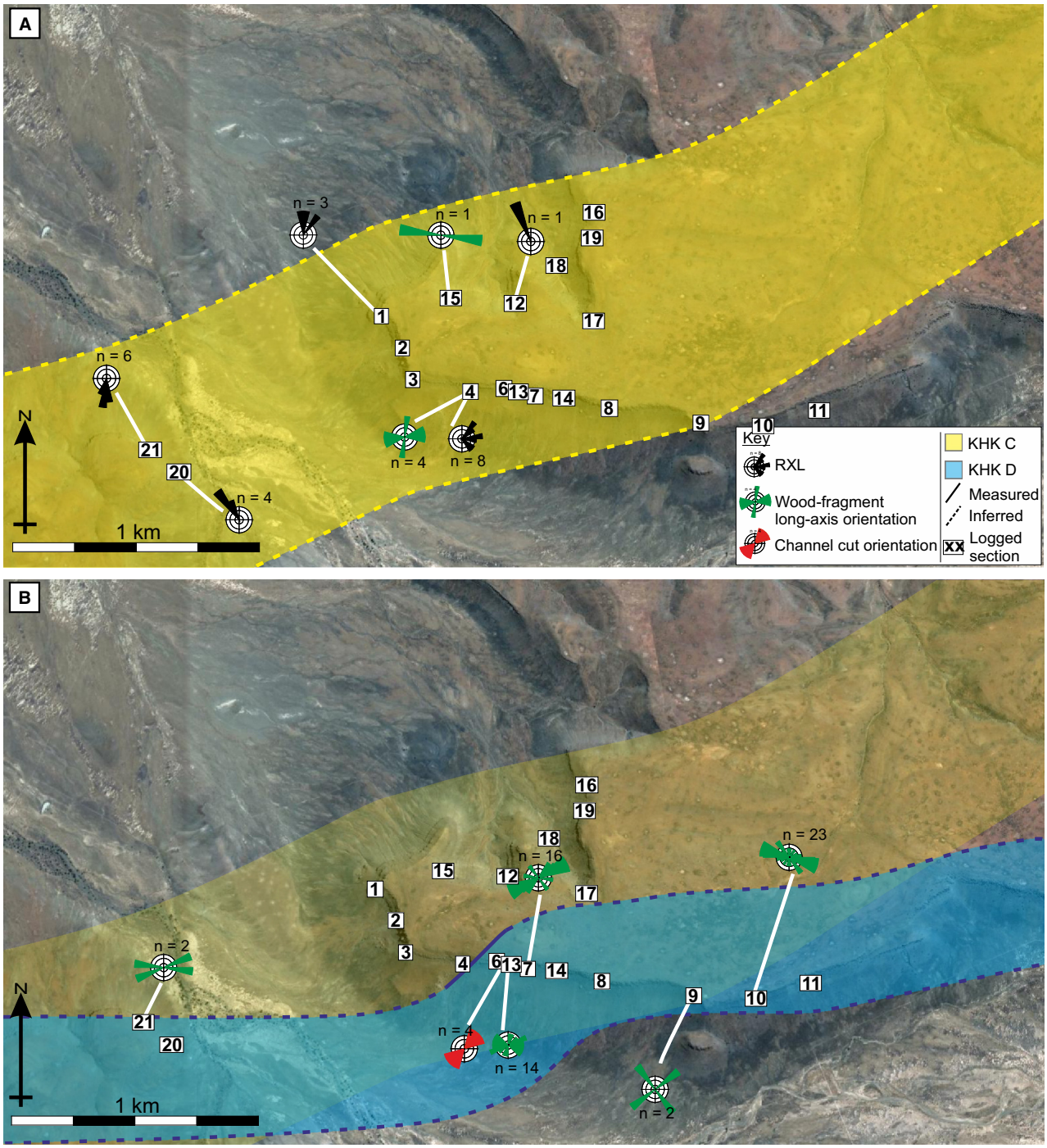

Fig. 10. Palaeocurrent data collected in the field. (A) KHKC is constrained by its outcrop limits, which are consistent with wood-fragment orientation. (B) The orientation of KHK is constrained by the channel-cut at Log 13 and its outcrop limits, which are supported by preferred wood-fragment orientations.

KHKC

Ripple cross-lamination measurements from Logs 1, 12 and 20 through KHKC suggest northward palaeoflow, whereas measurements from Logs 4 and 21 suggest southward and eastward palaeoflow, respectively (Fig. 10A). Long-axes of wood-fragments in Logs 4 and 15 are oriented east–west (Fig. 10A). The northward thinning of KHKC towards Logs 15, 16 and 18 (Fig. 6) suggests that the axis of the channel was situated

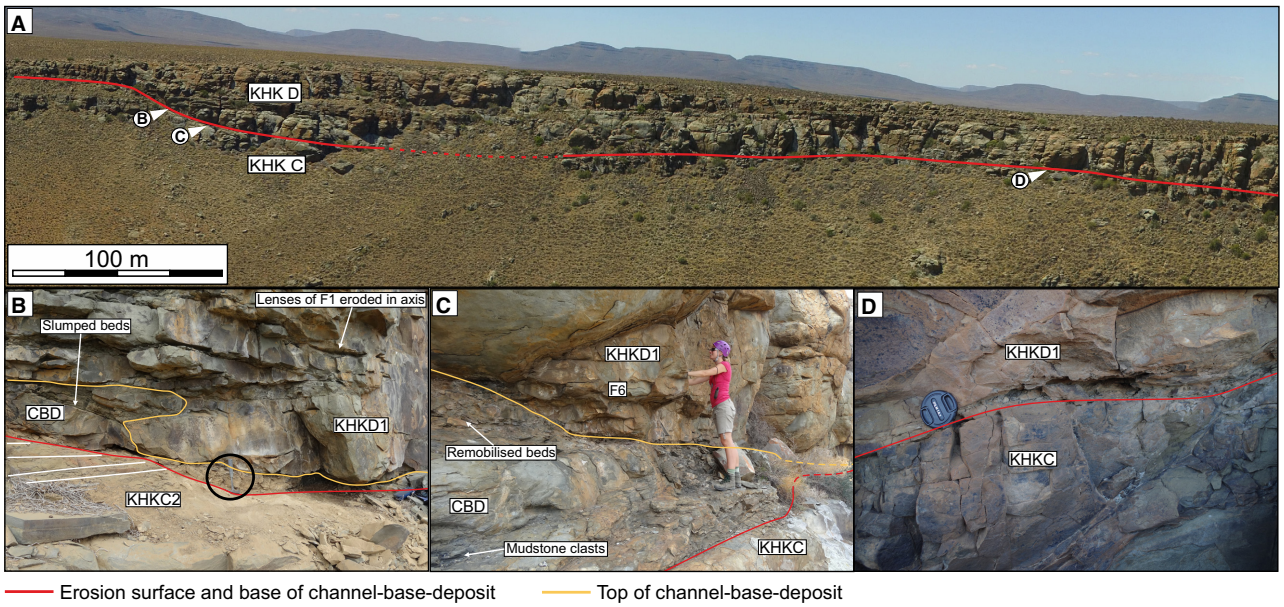

Fig. 11. Lateral variability in facies of the KHKD channel-base-deposit. (A) Unmanned aerial vehicle (UAV) photograph of KHK showing positions of (B), (C) and (D). (B) Channel complex scale channel-base-deposit in an off-axis position which comprises draping thin-bedded sandstones and slumped beds. Hammer circled (27 cm long). (C) Highly composite channel complex scale channel-base-deposit in a channel axis position of KHKD1. Person for scale is *ca* 1.8 m tall. (D) Sharp, mudstone-clast-rich amalgamated erosion surface between channel complexes KHKC and KHKD. Lens cap (60 mm diameter) for scale.

south of those localities (Fig. 10A). The absence of KHKC in south-eastern Logs 10 and 11 indicates that the channel was located to the north of these positions. Channel margin facies observed in channel elements C3 and C4 at Logs 4 and 5 suggest that the axis of these channel elements was positioned to the north (Figs 9 and 10A).

These data suggest that KHKC was oriented north-east/south-west, with a north-eastward palaeoflow consistent with regional palaeocurrent observations (e.g. Hansen *et al.*, 2019), and is essentially straight at the scale of the outcrop (Fig. 10A). Variable ripple cross-lamination trends are interpreted to represent flows that over-spilled the channel axis, and which may have been deflected off confining slopes (e.g. Kane *et al.,* 2010).

KHKD

The western margin of KHKD is well-constrained at Log 13, where the strike of the channel-cut is oriented north-east/south-west (Figs 9 and 10B). Long-axes of wood-fragments show preferred orientations to the east at Logs 13 and 20, and north-east at Log 7, respectively (Fig. 10B). At Log 11, the preferred wood-fragment orientation is east/south-east. The presence of KHKD at Logs 20 and 21, and eastward of Log 5, but absence at Logs 3 and 4, suggest that KHKD curved around these positions to the south (Figs 6 and 10B). The absence of KHKD in localities on the north face of Klein Hangklip suggests that the channel lay to the south (Figs 6 and 10B). Exposure of KHKD is continuous along the east–west oriented southern face, suggesting that the orientation of KHKD is parallel to sub-parallel to the outcrop (see Panel 1; Figs 2 and 10B). Log 10 contains a greater proportion of channel margin facies relative to Logs 9 and 11, which are both thicker, and show an increase in channel axis facies (F4b and F6) in their respective directions (Panel 1; Fig. 2B), suggesting that the channel margin is located to the south of these positions (Fig. 10B). The channel-cut and wood-fragment orientation at Logs 7 and 13 suggests that KHKD was sinuous at the scale of the outcrop (Fig. 10B). This is further supported by facies asymmetry at the western margin (e.g. Pyles *et al.,* 2010), and facies transitions between Logs 9, 10 and 11, which suggest that the channel axis curved around to the north of Log 10.

Channel architecture interpretations

Type-1: Low aspect ratio channel elements

KHKC1 and KHKC2, and KHKD1 and KHKD2, are the two lowermost channel elements in their respective channel complexes (Figs 6 and 8). Each channel element is thickest in the channel complex axis, thinning towards the margin of the channel complex, and incised into the underlying stratigraphy by 5.5 to 22.5 m (Figs 4 and 9). Basal erosion surfaces have gull-wing geometries, and are typically mantled by mudstone clasts in the channel axis, which decrease in abundance towards the channel margins (Figs 6, 7 and 11A to D). At the channel axes, channel-base-deposits are typically composite, forming packages up to 2.5 m thick, and consist of clast-rich siltstone, discontinuous argillaceous sandstones and locally remobilised beds (Fig. 11C). In off-axis positions, channel-base-deposits are more silt-rich with thin sandstone beds, and localised metre-scale slide blocks (Fig. 11B); locally the channel-base-deposit is preserved as a mudstone clast-rich amalgamation surface (Fig. 11D). At channel margin positions, the channel-base-deposit is characteristically represented by 0.5 to 0.3 m of siltstone. The channel axis of low aspect ratio channel elements is characterised by amalgamated F4b with localised F6 near the base, and F2 is sometimes observed in the upper few metres (Figs 6 and 8). Off-axis positions typically consist of F4a and F4b with increasing proportions of F2 towards the channel margin; F6 is rarely observed (Figs 6 and 8). The channel margins consist of F4a and F2 (Figs 6 and 8).

Type-2: High aspect ratio channel elements

KHKC3 and KHKC4, and KHKD3 and KHKD4 constitute the uppermost channel elements in their respective channel complexes (Figs 6 and 8). The channel elements are tabular in geometry and have comparatively high aspect ratios with relatively consistent thicknesses (typically 2 to 6 m), but locally have thicknesses between 1.2 m and 13 m (Figs 6 and 8). Basal erosion surfaces are typically tabular to subhorizontal and commonly mantled by mudstone clasts (Figs 7 and 9). The associated channel-base-deposit is typically 0.05 to 0.3 m of siltstone with localised mudstone clasts, though it may be present as an amalgamation surface marked by mudstone clasts. Channel axis deposits of high aspect ratio channel elements consist of bedded F4a and uncommon F4b, with localised F6 and F2 at the base and top, respectively (Figs 4 and 6). Off-axis positions comprise comparatively thinner-bedded F4a and F2 (Figs 4 and 6). Channel margin positions are characterised by a proportional increase in F2 (Figs 4 and 6). F1 and F3 are observed in KHKC4 in south-eastern localities (Fig. 6).

Channel element architecture

KHKC and KHKD are each composed of four channel elements; two low aspect ratio channel elements overlain by two high aspect ratio channel elements. Both channel complexes are high sand-to-gross, the minimum recorded value is 88.5% in KHKC at Log 15. All other logged sections have sand-to-gross values in excess of 90%.

KHKC. Palaeocurrent directions, outcrop geometries and facies transitions suggest that KHKC is relatively symmetrical and straight at the scale of the outcrop (Fig. 10A). The channel axis of each channel element in KHKC is situated in the channel complex axis (Fig. 6) suggesting aggradationally stacked channel elements with relatively symmetrical facies distribution. Channel margin positions are dominated by bedded F2 and F4a, with localised F1 and F3 (Figs 4 and 6). Off-axis positions are characterised by F2 and F4a, infrequent F4b and rare F6 (Figs 4 and 6). Channel axis positions are dominated by F6 and F4b in the lower, low aspect ratio channel elements, but comprise bedded F4a and F4b with localised F6, and an upward proportional increase in F2 (Figs 4 and 6).

KHKD. Palaeocurrents and outcrop geometries suggest that KHKD was sinuous at the scale of the outcrop (Fig. 10B). The channel-complex geometry is asymmetrical, with a steeper western channel cut and shallower eastern channel cut (Figs 8 and 9). Each channel element is thickest and contains respectively higher proportions of F6 and F4b in positions in the channel axis immediately east of the western channel cut (Figs 8 and 9). Facies transitions to channel margins dominated by F2 are gradual to the east, but comparatively abrupt to the west against the steeper channel cut (Figs 8 and 9). The asymmetrical channel element facies distribution suggests that the channel axes of successive channel elements were concentrated in the outer bank of the channel complex bend, and stacked aggradationally (Figs 8 and 9; see also

Navarro *et al.*, 2007; Jobe *et al.*, 2010; Labourdette & Bez, 2010; Pyles *et al.*, 2010; Li *et al.*, 2016). These relationships are strongest in low aspect ratio channel elements, D1 and D2 (Figs 8 and 9). The upper, high aspect ratio channel elements D3 and D4 exhibit more-laterally extensive deposits of F4a and F4b; however, F6 is only identified in the channel complex axis (Figs 8 and 9).

Distribution of channel-base-deposits

Low aspect ratio channel element channel-base-deposits typically have a relatively steep angular contact to underlying strata and exhibit facies asymmetry (for example, Figs 9 and 11). Channel axis positions are characterised by relatively thick composite channel-base-deposits (up to 2.5 m), comprising clast-rich siltstones, remobilised clasts of F4 and F6 up to 1.5 m in length, mudstone rafts and amalgamated packages of F6 (Fig. 11C). Locally, channel-base-deposits are not composite, and are identified only as clast-rich amalgamation surfaces with the sandstones of the underlying channel element (Figs 7C and 11C). Typically, off-axis positions exhibit a slightly thinner deposit and contain localised slumped beds that were shed from the channel erosion surface (Fig. 11B). Channel margin positions are characterised by <30 cm thick, locally clast-rich, siltstone deposits that typically overlie a mudstone-clast-rich bed top. KHKD2 differs from other low aspect ratio channel elements because it lacks a preserved channel-base-deposit (Fig. 7C). Instead, the subtle erosion surface is marked by a sharp, sub-parallel, facies transition from thin-bedded F4a to F4b (Fig. 7C).

High aspect ratio channel element channel-base-deposits are relatively flat-lying, are characterised by siltstones up to 40 cm thick, and are less heterogeneous compared to those of low-aspect ratio channel elements (Fig. 7E to H). Channel-base-deposits in channel axis positions frequently contain millimetre-scale to centimetre-scale clasts of siltstone and commonly overlie a mudstone-clast-rich bed top. Locally, the channel-base-deposit is marked by a clast-rich amalgamation surface. Channel off-axis and margin positions are comparatively clast-poor, although local beds of siltstone starved ripples are observed. The KHKD4 channel-base-deposit comprises 5 to 10 cm of thin-bedded coarse-siltstone to very fine-sandstone beds, and locally a <10 cm siltstone, which are subtly incised by overlying beds of the channel-fill (Fig. 7G and H). In contrast, the KHKD3 channel-base-deposit is locally composite adjacent to the steep KHKD channel-cut surface.

DISCUSSION

Stratigraphic evolution

Incision and the resultant development of a composite channel complex-set erosion surface is the first recorded phase of channel evolution (Figs 12A and 13). In common with other documented examples, the development of the surface is likely to have been time-transgressive (Sylvester *et al.*, 2011; Hodgson *et al.*, 2016; Englert *et al.*, 2020). However, the record of the development of the surface, and its formative processes, is obscured due to both the erosion of stratigraphy deposited during excavation of the surface, and the limited exposure of the surface and its channel-base-deposit. The 1.5 m thick channel-base-deposit mantling the channel complex set erosion surface (Fig. 7A and B) is interpreted to have been deposited from relatively dilute parts of multiple flows, which were primarily confined in the channel axis (e.g. Hubbard *et al.,* 2014). These deposits suggest that the erosion surface acted as a long-lived conduit for the bypass of sediment into the deeper basin (Fig. 13; e.g. Hubbard *et al.*, 2014; Stevenson *et al.*, 2015; Englert *et al.*, 2020). The nature of channel-base-deposits is used as a proxy for the energy, and number of, bypassing, partially bypassing, and depositional flows; and the relative durations of the complete sediment-bypass, bypass-dominated, and depositional phases (*sensu* Stevenson *et al.,* 2015). This approach assumes that the preserved deposit reflects the time-averaged flow-processes during deposition, and that any material that was deposited is preserved.

The fill of KHKC records the transition from complete sediment bypass to a depositional zone (*sensu* Stevenson *et al.,* 2015; Figs 12B and 13), relative to the channel axis. Aggradational phases are interpreted to be comparatively short-lived due to decreased evidence of erosion and reworking (see also Englert *et al.*, 2020). The first stage of this aggradation is recorded by the strongly channelised fill of C1 (Fig. 12B). A subsequent phase of incision and filling is marked by channel element C2 (Fig. 12C), indicating an increase in flow-energy, sediment bypass, and degradation of the slope (Fig. 13). Flows causing degradation of the slope were not necessarily larger (e.g.

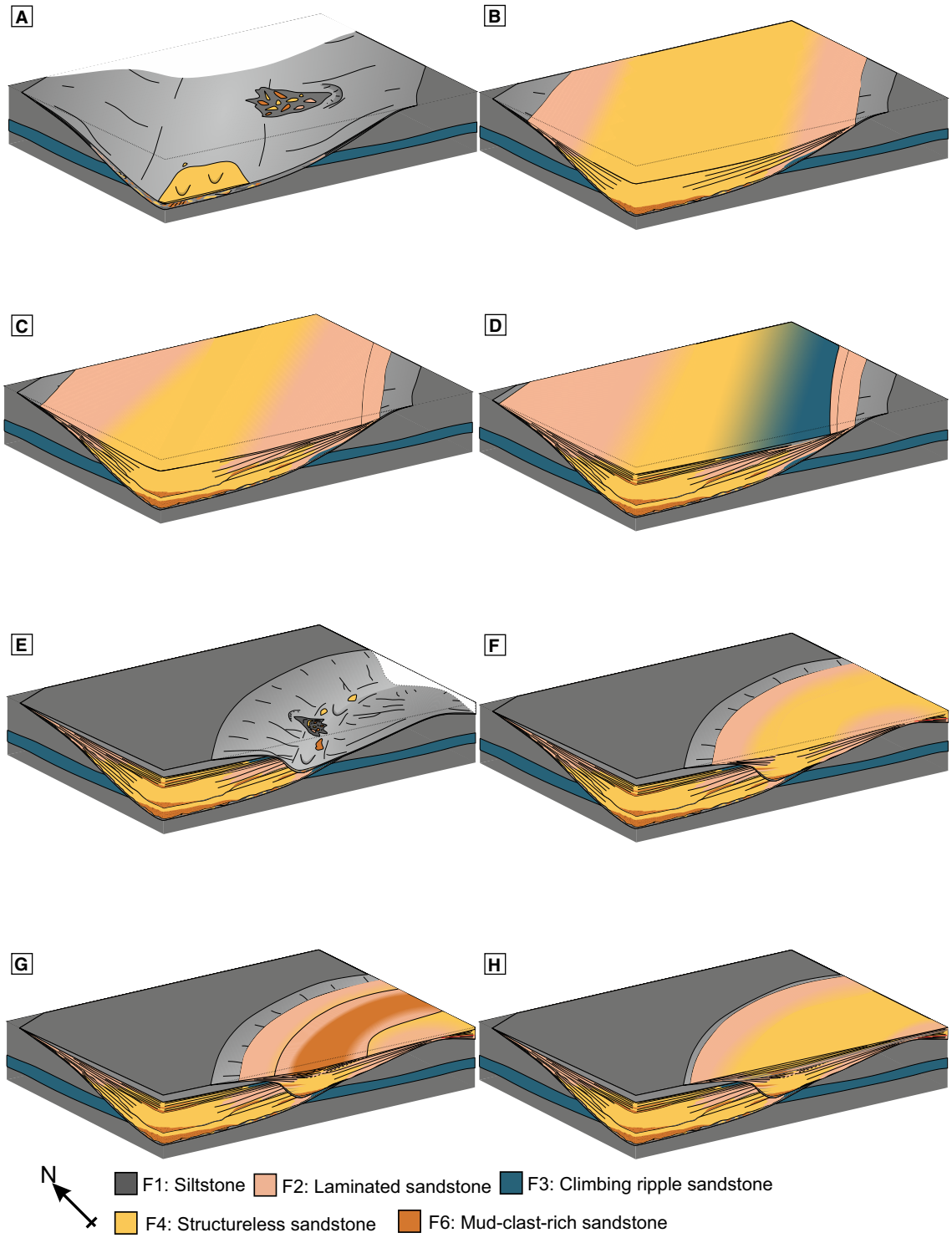

Fig. 12. Stratigraphic evolution of the KHK channel system. (A) Erosion of the KHKC surface and sediment bypass-dominated zone. (B) Transition to deposition dominated flows and infilling of KHKC1. (C) Incision and subsequent infilling of KHKD2. (D) Shallow incision and infill of high aspect ratio channel elements KHKC3 and KHKC4. (E) Sediment bypass-dominated zone resulting in excavation of KHKD channel cut. (F) Transition to deposition dominated flows and aggradation of KHKD1. (G) Incision and fill of KHKD2. (H) Shallow incision and deposition of the KHKD3 and KHKD4 channel elements.

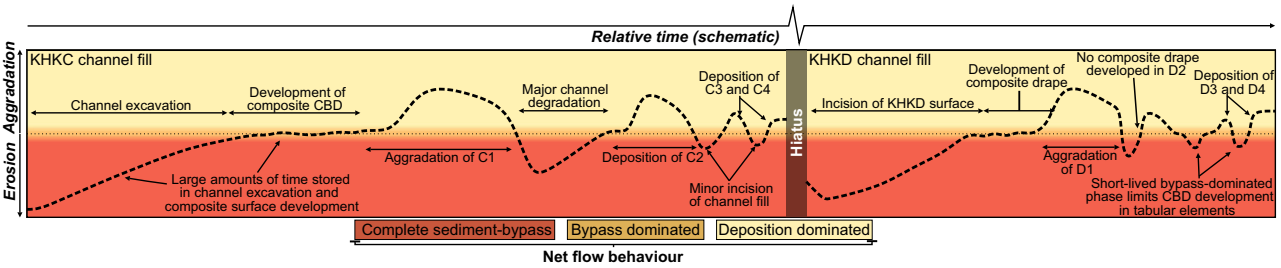

Fig. 13. Schematic illustration of channel evolution and flow behaviour in the channel axis of respective channel complexes. Highly composite erosion surfaces and channel-base-deposits suggest the excavation of channel cuts and bypass phases record long periods of time. However, most of the thickness of the channel-fill is represented by aggradational sandstones developed under strongly depositional flows. This suggests that time-partitioning in submarine channels may be biased towards individual surfaces, which occupy a small portion of the channel thickness.

Sylvester *et al.,* 2011), but were more erosive than flows resulting in aggradation. The C2 channel-base-deposit is highly composite, suggesting that there was a long-lived bypass-dominated zone before aggradation of the C2 fill (Fig. 13). The individual fills of C1 and C2 record a vertical decrease in evidence for sediment bypass up stratigraphy (Fig. 13), from F6 and F4b at the base to F2 and F4a at the tops (Figs 4 and 6).

The upper-fill of C2 was partially incised during the formation of the higher aspect-ratio channel element C3, indicating an increase in flow energy, erosion, and sediment bypass (Figs 12D and 13). The C3 fill was also partially incised as part of the development of channel element C4. The thin siltstone-rich channel-base-deposits, shallow depth of incision and less-composite nature suggest that erosion and bypass was less-pronounced and protracted, probably due to less-erosive flows, compared to the incisions related to C1 and C2 (Fig. 13). The fills of C3 and C4 are similar and suggest a temporal decrease in flow energy (Figs 12D and 13).

Following the fill of the KHKC channel complex, approximately 2 m of siltstone was deposited, representing a prolonged hiatus of sand supply to the area. The period of silt-prone deposition was ended by incision of the KHKD channel-cut (Fig. 12E) indicating an increase in flow energy and sediment bypass (Fig. 13; e.g. Kneller, 2003); possibly driven by eustatic sea-level fall (e.g. Flint *et al.,* 2011) and the overall progradation of the system (e.g. Hodgson *et al.,* 2006). The highly composite channel-base-deposit includes depositional and erosional features at the base of the D1 channel axis, suggesting that the channel axis was a long-lived sediment bypass zone (Fig. 13; e.g. Hubbard *et al.,* 2014; Stevenson *et al.,* 2015).

A gradual transition to net depositional flows resulted in the fill of the KHKD channel complex (Figs 12F and 13). KHKD1 records an upward decrease in in F6 and bed amalgamation, supporting a temporal reduction in sediment bypass (Figs 12F and 13). Facies asymmetry, with F6 and F4b being more common adjacent to the steep western channel-cut (Fig. 12F), suggests that the highest energy flow components were located near the base of the outer-bank (secondary or helical flow; see Keevil *et al.,* 2006; Imran *et al.,* 2007; Peakall *et al.,* 2007; Peakall & Sumner, 2015). Erosion of F1 lenses from the channel-cut in towards the channel axis (Fig. 11B and C) suggests that flows were highly energetic in the thalweg of the channel axis (Reimchen *et al.,* 2016), and decelerated against the outer channel-cut (e.g. Keevil *et al.,* 2006).

The incision related to the fill of D2 (Fig. 7C) is interpreted to represent erosion by bypassing flows. The channel-base-deposit related to D2 is sharp and non-composite, suggesting a short-lived bypass-dominated phase, or that subsequent flows eroded the initial channel-base-deposit (Fig. 13). The D2 fill records aggradation of the channel fill by lower energy, depositional flows (Fig. 13). However, the upper fill of D2 contains scours, which were infilled by thin beds. This may be associated with a gradual increase in flow energy, and record the transition from depositional, to partially bypassing, to fully bypassing flows, which resulted in the incision of the D3 channel-cut (Figs 12G and 13; see also package 2 of Pyles *et al.,* 2010). The upper part of D2 is weakly incised, considered to reflect a decrease in flow energy and sediment bypass compared to the incision of underlying channel elements (Fig. 13). The lack of incision and composite channel-base-deposits suggests

that the amount, and subsequent duration, of sediment bypass was limited (Fig. 13). The channel-base-deposit is overlain by high aspect ratio channel element D3 (Fig. 12H), indicating that flows became deposition-dominated (Fig. 13). The fill of the D3 channel element was incised as part of the development of channel element D4 (Figs 12H and 13). The incision surface of D4 is relatively flat-lying compared to low aspect ratio channel elements, suggesting limited phases of bypassing and partially bypassing flows (Fig. 13). However, the channel-base-deposit is locally composite in the area adjacent to the steep channel-cut of KHKD, which is located on the outer bend of the channel. This suggests that higher-energy parts of flows were concentrated at the outer bend, and that bypass and substrate remobilisation was more efficient in these locations. The subsequent aggradation of the D4 channel element reflects the transition to depositional flows (Fig. 13).

Three-dimensional channel architecture

The KHK outcrop permits quasi-3D facies distribution to be recorded in a series of depositional dip-oriented and strike-oriented panels (Figs 6 and 8). The KHKC channel complex shows no substantial down depositional-dip changes in geometry or sandstone to gross. However, subtle changes in facies are recorded in dip-oriented sections, from F4 to F2 to F4, and varying thickness and distribution of F6 (Figs 4 and 6). The KHKC channel complex is interpreted to be relatively straight at the scale of the outcrop. Channel complex KHKD, which is inferred to be sinuous in planform, has a steeper western (outer-bank) channel cut, and displays a more pronounced facies variation across depositional-strike with a greater proportion of F4b and F6 compared to the eastern side of the channel cut. These observations are made on a 0.1 to 1.0 km scale, in predominantly sandstone-filled channels; similar distributions have been noted in other channel systems such as the Beacon Channel (Pyles *et al.*, 2010). However, at a system-scale (i.e. over tens to hundreds of kilometres), channel-fills may show major longitudinal facies variability in response to the dominance of different flow processes. In proximal areas, slumps and debris flows are more abundant, whereas in distal parts of the system deposits of high-density and low-density turbidites are more commonly observed (De Ruig & Hubbard, 2006; Malkowski *et al.,* 2018). Therefore, at the scale of the depositional system, flow processes, and the methods of sediment mobilisation in up-dip areas are likely to have the strongest influence on heterogeneity. Channel sinuosity, and its effect on the inherited flow processes, is likely to determine local facies distribution and channel element geometries over longitudinal profiles of 0.1 to 1.0 km (e.g. De Ruig & Hubbard, 2006; Pyles *et al.,* 2010; Reimchen *et al.,* 2016; Malkowski *et al.,* 2018).

Controls on channel element architecture

Each channel complex contains two low aspect ratio channel elements overlain by two high aspect ratio channel elements. Low aspect ratio channel elements have lenticular geometries and facies distributions, with bed thicknesses that decrease from channel axis to channel margin. Highly erosive flows are interpreted to have incised the basal channel-cuts (Fig. 13; Pyles *et al.,* 2010; McHargue *et al.,* 2011; Fildani *et al.,* 2013; Hubbard *et al.,* 2014; Hodgson *et al.,* 2016). Subsequently flows became progressively confined, enhancing flow efficiency (*sensu* Mutti, 1992), increasing bypass and erosion, and further entrenching the channel (e.g. Hodgson *et al.,* 2016). Development of thick, composite channel-base-deposits (Figs 7A, 11B and 11C) is interpreted to represent a prolonged sediment bypass-dominated period in the channel axis through the early stages of waning sediment supply (Fig. 13; e.g. Hubbard *et al.,* 2014). This early stage of channel aggradation was likely characterised by numerous flows which were bypassing, partially bypassing and depositional. The gradual transition to net depositional flows is preserved in the channel-base-deposit where deposits of earlier depositional flows were eroded and remobilised by bypassing or partially bypassing flows (see also Vendettuoli *et al.,* 2019). Remobilised deposits and clasts of beds (Fig. 11B and C) suggest that successive flows were transitional between depositional, and fully bypassing, remobilising beds (Fig. 13; e.g. Stevenson *et al.,* 2015). This is possibly linked to smaller cycles of waxing and waning energy superimposed on the overall trend (e.g. Vendettuoli *et al.,* 2019). KHKD2 differs from other low aspect ratio channel elements as it lacks a composite channel-base-deposit (Fig. 7C). The subtle, amalgamated KHKD2 channel-base-deposit surface is interpreted to represent either: (i) a relatively rapid transition from near-complete sediment bypass to deposition-dominated flows, inhibiting the development of a composite channel-base-deposit (Fig. 13); or (ii) incision

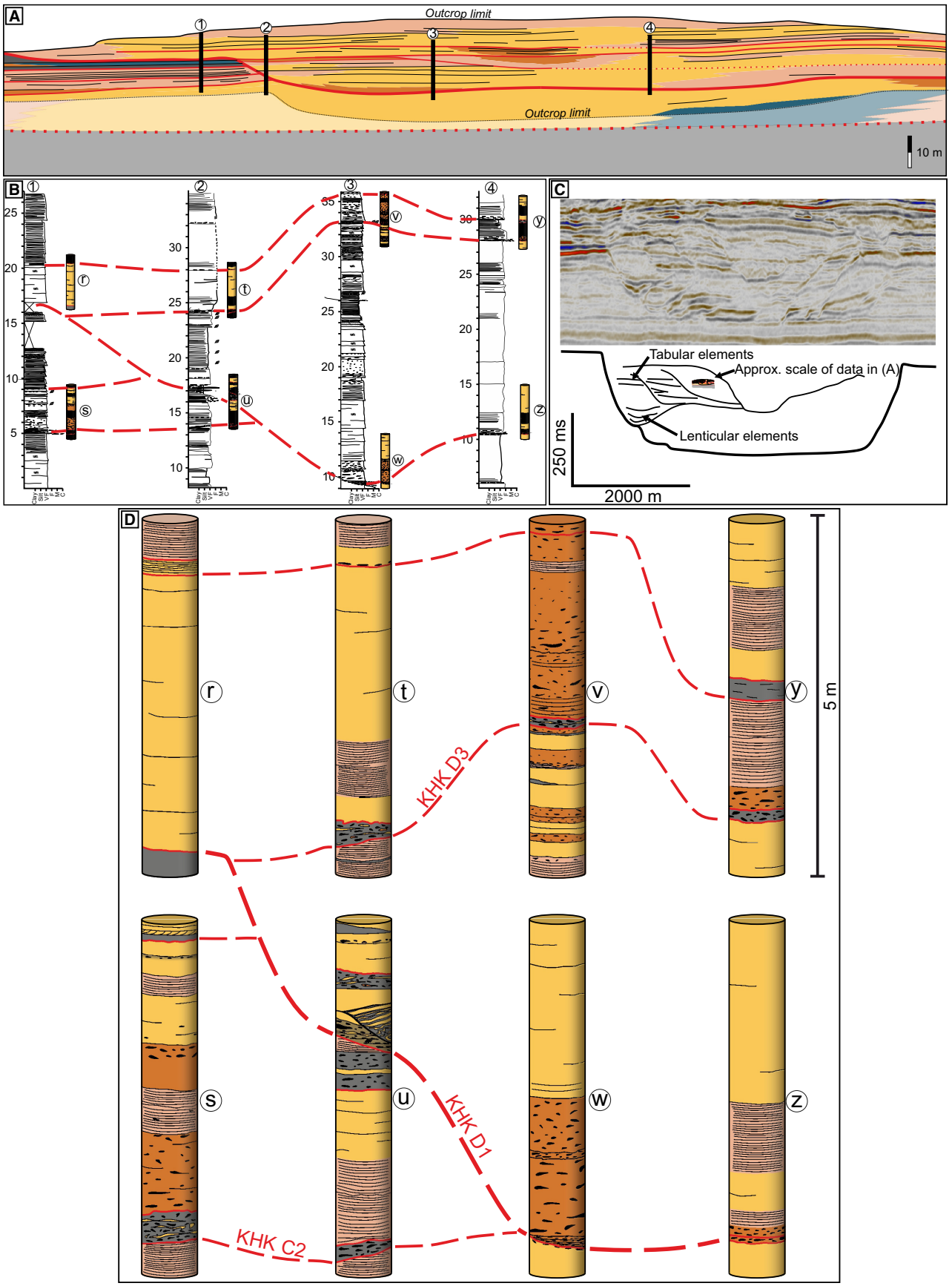

Fig. 14. Comparison of scales of observation. (A) Photopanel interpretation of the Klein Hangklip outcrop. (B) Sedimentary logs collected from the outcrop, with key surface interpretations. (C) Comparison to a Miocene channel complex set from the Taranaki Basin, New Zealand. The Klein Hangklip channel-fills, and the heterogeneities within them are 1 to 2 reflectors thick. Data sourced from the New Zealand Petroleum and Minerals Petroleum Exploration Dataset. (D) Synthetic cores, drawn from logged data, of key stratigraphic positions illustrating the challenges of correctly identifying key channel surfaces in one-dimensional datasets. Red dashed lines represent erosion surfaces.

and erosion of the initial channel-base-deposit by later flows.

A gradual upward increase in the number of net depositional flows resulted in initial aggradation and deposition of amalgamated F6 at the base of the channel complex axis (Fig. 13). Packages of F6 overlain by F4 at the base of channel-fills are interpreted to record the transition from bypassing, to partially bypassing, to depositional flows. During aggradation, higher-concentration flows, or parts of flows, were more strongly influenced by channel topography, and were contained in the channel axis where they rapidly deposited thick packages of F4b (e.g. Hubbard *et al.,* 2014). Local changes in intra-channel topography and gradient may have resulted in subtle down-dip and across-strike variations in depositional facies caused by flow acceleration or deceleration, and entrainment of substrate. Dilute, low-concentration flow components were able to surmount channel topography to the channel margins, depositing thinner bedded F4a and F2 (Fig. 12; e.g. Campion *et al.,* 2000; Jobe *et al.*, 2017). Disparity in deposit thickness resulted in more rapid fill of accommodation in the channel axis relative to the channel margin (see also: Hubbard *et al.,* 2014).

Subsurface implications

Seismic reflection data do not have the vertical resolution to show complicated geometric relationships and small-scale features such as channel-base-deposits (Fig. 14; e.g. Alpak *et al.,* 2013; Morris *et al.,* 2016). Therefore, well-data are crucial in identifying these features in the subsurface in order to build realistic geological models. The Klein Hangklip seismic-scale channel-fill has a high sand percentage, typically in excess of 90%. In such a channel-fill, the heterogeneities controlling reservoir performance are likely to be related to sandstone facies and depositional processes (e.g. Hirst *et al.*, 2002; Lien *et al.*, 2006; Zhang *et al.*, 2015; Porten *et al.*, 2016; Bell *et al.*, 2018), and the distribution and character of channel-base-deposits (Larue & Hovadik, 2006; Funk *et al.*, 2012; Alpak *et al.*, 2013; Jackson *et al.*, 2019).

Core logging and image log/dip-meter analysis are common ways to identify and interpret channel-base-deposits and erosion surfaces (e.g. Barton *et al.,* 2010; Morris *et al.,* 2016). This study reveals that these methods may prove challenging as:

1 Highly composite channel-base-deposits are locally observed as clast-rich amalgamation surfaces, not suggestive of substantial sediment bypass (Figs 11 and 14). Thus, small changes in well placement could result in dramatically different core interpretations (Fig. 14).

2 Siltstone bypass channel-base-deposits may be challenging to differentiate from abandonment or low-energy depositional drapes without identification of clasts or a mudstone-clast-rich basal surface (Fig. 14), which may influence the prediction of reservoir sandstones down-dip.

3 Some erosion surfaces are characterised by subtle amalgamation surfaces and facies changes, which may not be interpreted as a major bounding surface (Figs 7, 11 and 14).

4 High aspect ratio channel elements have relatively flat-lying erosion surfaces, which may make dip-meter identification challenging (Fig. 14).

CONCLUSIONS

The Klein Hangklip outcrop of Unit 5 of the Skoorsteenberg Formation permits high-resolution analysis of the architecture, facies and stacking patterns of a submarine slope channel complex set, composed of two stacked channel complexes. The lower channel-complex, which is 32.9 m thick and at least 890 m wide, is straight at the scale of the outcrop; the upper channel-complex is 39.0 m thick, is sinuous, and exhibits architectural and facies asymmetry.

Each channel-complex consists of four channel-elements, which are grouped into:

1 Lower channel-elements which are: (i) low-aspect ratio; (ii) incise up to 20 m into underlying stratigraphy; and (iii) exhibit strong facies trends from abundant amalgamated structureless sandstone and mudstone-clast-rich facies in channel-axis positions to bedded structureless sandstone and laminated sandstones in channel-margin positions.

2 Upper-channel elements are: (i) high-aspect ratio; (ii) do not incise deeply into underlying stratigraphy; and (iii) have less-contrasting channel-axis to channel-margin facies transitions.

In both channel complexes systematic and predictable facies changes are observed from comparatively thick-bedded amalgamated sandstones deposited from energetic flows in channel-axis positions, to bedded and laminated sandstones in channel-margin positions. Conversely, positions in comparative down-depositional dip positions (for example, from an up-dip channel axis position to a down-dip channel axis position) show subtle, but non-systematic heterogeneity in sandstone facies.

Channel-base-deposits mapped in depositional-dip and strike sections exhibit spatial and temporal heterogeneity at metres to hundreds of metres length scales, which could inhibit accurate characterisation in subsurface and limited-outcrop studies. The depth of incision and composite nature of channel-base-deposits are used as proxies for the existence of long-lived bypass conduits. This analysis suggests that time-partitioning during channel evolution is strongly biased towards excavation and maintenance of these conduits, whereas aggradation of the relatively thick-bedded sandstone-fills was comparatively short-lived.

ACKNOWLEDGEMENTS

The authors thank the landowners for permission to access the study area. We are grateful to Kévin Boulesteix, Hannah Brooks, and Dave Lee for their assistance in the field. Editor Peir Pufahl and Associate Editor Jaco Baas are thanked for their constructive comments and handling of the manuscript. Emma Morris and an anonymous reviewer are thanked, whose points enhanced the clarity and readability of the manuscript.

DATA AVAILABILITY STATEMENT

Research data are not shared.

REFERENCES

Allen, J.R.L. (1970a) The sequence of sedimentary structures in turbidites, with special reference to dunes. *Scot. J. Geol.*, **6**, 146–161.

Allen, J.R.L. (1970b) A quantitative model of climbing ripples and their cross-laminated deposits. *Sedimentology*, **14**, 5–26.

Allen, J.R.L. (1982) *Sedimentary Structures*, Vol. **1–2**. Elsevier, Amsterdam, 592 pp.

Allen, J.R.L. (1991) The Bouma division A and the possible duration of turbidity currents. *J. Sed. Res.*, **61**, 291–295.

Alpak, F.O., **Barton, M.D.** and **Naruk, S.J.** (2013) The impact of fine-scale turbidite channel architecture on deep-water reservoir performance. *AAPG Bull.*, **97**, 251–284.

Altinakar, M.S., **Graf, W.H.** and **Hopfinger, E.J.** (1996) Flow structure in turbidity currents. *J. Hydraul. Res.*, **34**, 713–718.

Baas, J.H. (1994) A flume study on the development and equilibrium morphology of current ripples in very fine sand. *Sedimentology*, **41**, 185–209.

Baas, J.H. (1999) An empirical model for the development and equilibrium morphology of current ripples in fine sand. *Sedimentology*, **46**, 123–138.

Baas, J.H. and **Best, J.L.** (2002) Turbulence modulation in clay-rich sediment-laden flows and some implications for sediment deposition. *J. Sed. Res.*, **72**, 336–340.

Baas, J.H., **van Dam, R.L.** and **Storms, J.E.A.** (2000) Duration of deposition from decelerating high-density turbidity currents. *Sed. Geol.*, **136**, 71–88.

Baas, J.H., **Van Kesteren, W.** and **Postma, G.** (2004) Deposits of depletive high-density turbidity currents: a flume analogue of bed geometry, structure and texture. *Sedimentology*, **51**, 1053–1088.

Baas, J.H., **Best, J.L.**, **Peakall, J.** and **Wang, M.** (2009) A phase diagram for turbulent, transitional, and laminar clay suspension flows. *J. Sed. Res.*, **79**, 162–183.

Baas, J.H., **Best, J.L.** and **Peakall, J.** (2011) Depositional processes, bedform development and hybrid bed formation in rapidly decelerated cohesive (mud-sand) sediment flows. *Sedimentology*, **58**, 1953–1987.

Bain, H.A. and **Hubbard, S.M.** (2016) Stratigraphic evolution of a long-lived submarine channel system in the Late Cretaceous Nanaimo Group, British Columbia, Canada. *Sed. Geol.*, **337**, 113–132.

Bakke, K., **Gjelberg, J.** and **Agerlin Petersen, S.** (2008) Compound seismic modelling of the Ainsa II turbidite system, Spain: Application to deep-water channel systems offshore Angola. *Mar. Petrol. Geol.*, **25**, 1058–1073.

Bakke, K., **Kane, I.A.**, **Martinsen, O.J.**, **Petersen, S.A.**, **Johansen, T.A.**, **Hustoft, S.**, **Jacobsen, F.H.** and **Groth, A.** (2013) Seismic modeling in the analysis of deep-water sandstone termination styles. *AAPG Bull.*, **97**, 1395–1419.

Barton, M., **O'Byrne, C.**, **Pirmez, C.**, **Prather, B.**, **van, Der Vlugt, F.**, **Alpak, F.O.** and **Sylvester, Z.** (2010) Turbidite channel architecture: recognizing and quantifying the distribution of channel-base drapes using core and dipmeter data. In: *Dipmeter and Borehole Image Log Technology* (Eds. Pöppelreiter, M., García-Carballido, C. and Kraaijveld, M.), *AAPG Mem.*, **92**, 195–210.

Bayliss, N.J. and **Pickering, K.T.** (2015) Deep-marine structurally confined channelised sandy fans: Middle Eocene Morillo System, Ainsa Basin, Spanish Pyrenees. *Earth Sci. Rev.*, **144**, 82–106.

Beaubouef, R.T. (2004) Deep-water leveed-channel complexes of the Cerro Toro Formation, Upper Cretaceous, southern Chile. *AAPG Bull.*, **88**, 1471–1500.

Bell, D., **Kane, I.A.**, **Pontén, A.S.M.**, **Flint, S.S.**, **Hodgson, D.M.** and **Barrett, B.J.** (2018) Spatial variability in depositional reservoir quality of deep-water channel-fill and lobe deposits. *Mar. Petrol. Geol.*, **98**, 97–115.

Best, J.L. and **Bridge, J.S.** (1992) The morphology and dynamics of low amplitude bedwaves upon upper stage plane beds and the preservation of planar laminae. *Sedimentology*, **39**, 737–752.

Boulesteix, K., **Poyatos-Moré, M.**, **Flint, S.S.**, **Taylor, K.G.**, **Hodgson, D.M.** and **Hasiotis, S.T.** (2019) Transport and deposition of mud in deep-water environments: Processes and stratigraphic implications. *Sedimentology*, **66**, 2894–2925.

Bouma, A.H. (1962) Sedimentology of Some Flysch Deposits: A Graphic Approach to Facies Interpretation. Elsevier, Amsterdam 168p.

Bouma, A.H. (2000) Coarse-grained and fine-grained turbidite systems as end member models: applicability and dangers. *Mar. Petrol. Geol.*, **17**, 137–143.

Bouma, A.H. and **Wickens, H. de V.** (1991) Permian passive margin submarine fan complex, Karoo Basin, South Africa: Possible model to Gulf of Mexico. *Gulf Coast Assoc. Geol. Soc.*, **41**, 30–42.

Bouma, A.H. and **Wickens, H. de V.** (1994) Tanqua Karoo, ancient analog for fine-grained submarine fans. In: *Submarine Fans and Turbidite Systems—Sequence Stratigraphy, Reservoir Architecture and Production Characteristics Gulf of Mexico and International* (Eds Weimer, P., Bouma, A.H. and Perkins, B.F.), *Geol. Soc. Am.,* 23–34.

Bruhn, C.H.L. and **Walker, R.G.** (1997) Internal architecture and sedimentary evolution of coarse-grained, turbidite channel-levee complexes, early eocene regência canyon, Espirito Santo Basin, Brazil. *Sedimentology*, **44**, 17–46.

Bryant, I.D. and **Flint, S.S.** (1993) Quantitative clastic reservoir geological modelling: problems and perspectives. *The Geological Modelling of Hydrocarbon Reservoirs and Outcrop Analogues. Int. Assoc. Sedimentol. Spec. Publ.*, **15**, 3–20.

Butler, R.W.H. and **Tavarnelli, E.** (2006) The structure and kinematics of substrate entrainment into high-concentration sandy turbidites: a field example from the Gorgoglione 'flysch' of southern Italy. *Sedimentology*, **53**, 655–670.

Campion, K.M., **Sprague, A.R.**, **Mohrig, D.**, **Lovell, R.W.**, **Drzewiecki, P.A.**, **Sullivan, M.D.**, **Ardill, J.A.**, **Jensen, G.N.** and **Sickafoose, D.K.** (2000) Outcrop expression of confined channel complexes. In: *Deep-Water Reservoirs of the World: SEPM, Gulf Coast Section, 20th Annual Research Conference* (Eds. Weimar, P., Slatt, R.M., Coleman, J., Rosen, N.C., Nelson, H., Bouma, A.H., Styzen, M.J. and Lawrence, D.T.), 127–151.

Casciano, C.I., **Patacci, M.**, **Longhitano, S.G.**, **Tropeano, M.**, **McCaffrey, W.D.** and **Di Celma, C.** (2019) Multi-scale analysis of a migrating submarine channel system in a tectonically-confined basin: The Miocene Gorgoglione Flysch Formation, southern Italy. *Sedimentology*, **66**, 205–240.

Castelltort, S., **Honegger, L.**, **Adatte, T.**, **Clark, J.D.**, **Puigdefàbregas, C.**, **Spangenberg, J.E.**, **Dykstra, M.L.** and **Fildani, A.** (2017) Detecting eustatic and tectonic signals with carbon isotopes in deep-marine strata, Eocene Ainsa Basin, Spanish Pyrenees. *Geology*, **45**, 707–710.

Clark, I.R. and **Cartwright, J.** (2009) Interactions between submarine channel systems and deformation in deepwater fold belts: Examples from the Levant Basin, Eastern Mediterranean sea. *Mar. Petrol. Geol.*, **26**, 1465–1482.

Clark, J.D. and **Pickering, K.T.** (1996) Architectural elements and growth patterns of submarine channels: Application to hydrocarbon exploration. *AAPG Bull.*, **80**, 194–221.

Covault, J.A. and **Graham, S.A.** (2010) Submarine fans at all sea-level stands: Tectono-morphologic and climatic controls on terrigenous sediment delivery to the deep sea. *Geology*, **38**, 939–942.

De Ruig, M.J. and **Hubbard, S.M.** (2006) Seismic facies and reservoir characteristics of a deep-marine channel belt in the Molasse foreland basin, Puchkirchen Formation, Austria. *AAPG Bull.*, **90**, 735–752.

De Wit, M.J. and **Ransome, I.G.D.** (1992) Regional inversion tectonics along the southern margin of Gondwana. In: *Inversion Tectonics of the Cape Fold Belt, Karoo and Cretaceous Basins of Southern Africa* (Eds De Wit, M.J. and Ransome, I.G.D.), pp. 15–21. Balkema, Rotterdam.

Di Celma, C.N., **Brunt, R.L.**, **Hodgson, D.M.**, **Flint, S.S.** and **Kavanagh, J.P.** (2011) Spatial and Temporal Evolution of a Permian Submarine Slope Channel-Levee System, Karoo Basin, South Africa. *J. Sed. Res.*, **81**, 579–599.

Dzulynski, S. and **Sanders, J.E.** (1962) Current marks on firm mud bottoms. *Trans. Connecticut Acad. Arts Sci.*, **42**, 58–96.

Englert, R.G., **Hubbard, S.M.**, **Matthews, W.A.**, **Coutts, D.S.** and **Covault, J.A.** (2020) The evolution of submarine slope-channel systems: Timing of incision, bypass, and aggradation in Late Cretaceous Nanaimo Group channel-system strata, British Columbia, Canada. *Geosphere*, **16**, 281–296.

Eschard, R., **Albouy, E.**, **Deschamps, R.**, **Euzen, T.** and **Ayub, A.** (2003) Downstream evolution of turbiditic channel complexes in the Pab Range outcrops (Maastrichtian, Pakistan). *Mar. Petrol. Geol.*, **20**, 691–710.

Fildani, A., **Hubbard, S.M.**, **Covault, J.A.**, **Maier, K.L.**, **Romans, B.W.**, **Traer, M.** and **Rowland, J.C.** (2013) Erosion at inception of deep-sea channels. *Mar. Petrol. Geol.*, **41**, 48–61.

Flint, S.S., **Hodgson, D.M.**, **Sprague, A. R.**, **Brunt, R.L.**, **der, Van Merwe, W.C.**, **Figueiredo, J.**, **Prélat, A.**, **Box, D.**, **Di Celma, C.** and **Kavanagh, J.P.** (2011) Depositional architecture and sequence stratigraphy of the Karoo basin floor to shelf edge succession, Laingsburg depocentre, South Africa. *Mar. Petrol. Geol.*, **28**, 658–674.

Fonnesu, M., **Patacci, M.**, **Haughton, P.D.W.** and **Felletti, F.** (2016) Hybrid event beds generated by local substrate delamination on a confined-baisn floor. *J. Sed. Res.*, **86**, 929–943.

Friend, P.F., **Slater, M.J.** and **Williams, R.C.** (1979) Vertical and lateral building of river sandstone bodies, Ebro Basin, Spain. *J. Geol. Soc. London*, **136**, 39–46.

Funk, J.E., **Slatt, R.M.** and **Pyles, D.R.** (2012) Quantification of static connectivity between deep-water channels and stratigraphically adjacent architectural elements using outcrop analogs. *AAPG Bull.*, **96**, 277–300.

Galy, V., **France-Lanord, C.**, **Beyssac, O.**, **Faure, P.**, **Kudrass, H.** and **Palhol, F.** (2007) Efficient organic carbon burial in the Bengal fan sustained by the Himalayan erosional system. *Nature*, **450**, 407.

Goldhammer, R.K., **Wickens, H. deV.**, **Bouma, A.H.** and **Wach, G.** (2000) Sequence stratigraphic architecture of the

late Permian Tanqua submarine fan complex, Karoo Basin, South Africa. In: *Fine-Grained Turbidite Systems: AAPG Mem. 72* (Eds. Bouma, A.H. and Stone, C.G.), *SEPM Spec. Publ.*, **68**, 165–172.

Gonzalez-Yajimovich, O.E., **Gorsline, D.S.** and **Douglas, R.G.** (2007) Frequency and sources of basin floor turbidites in alfonso basin, Gulf of California, Mexico: Products of slope failures. *Sed. Geol.*, **199**, 91–105.

Gwiazda, R., **Paull, C.K.**, **Ussler, W.** and **Alexander, C.R.** (2015) Evidence of modern fine-grained sediment accumulation in the Monterey Fan from measurements of the pesticide DDT and its metabolites. *Mar. Geol.*, **363**, 125–133.

Hansen, L.A.S., **Callow, R.H.T.**, **Kane, I.A.**, **Gamberi, F.**, **Rovere, M.**, **Cronin, B.T.** and **Kneller, B.C.** (2015) Genesis and character of thin-bedded turbidites associated with submarine channels. *Mar. Petrol. Geol.*, **67**, 852–879.

Hansen, L.A.S., **Hodgson, D.M.**, **Pontén, A.**, **Bell, D.** and **Flint, S.** (2019) Quantification of basin-floor fan pinchouts: Examples from the Karoo Basin, South Africa. *Front. Earth Sci.*, **7**, 12.

Haughton, P.D.W., **Barker, S.P.** and **McCaffrey, W.D.** (2003) Linked debrites in sand-rich turbidite systems - origin and significance. *Sedimentology*, **50**, 459–482.

Haughton, P.D.W., **Davis, C.**, **McCaffrey, W.** and **Barker, S.** (2009) Hybrid sediment gravity flow deposits – Classification, origin and significance. *Mar. Petrol. Geol.*, **26**, 1900–1918.

Hirst, J.P.P. (2012) Ordovician proglacial sediments in Algeria: insights into the controls on hydrocarbon reservoirs in the In Amenas field, Illizi Basin. *Geol. Soc. London. Spec. Publ.*, **368**, 319–353.

Hirst, J.P.P., **Benbakir, A.**, **Payne, D.F.** and **Westlake, I.R.** (2002) Tunnel valleys and density flow processes in the Upper Ordovician glacial succession, Illizi Basin, Algeria: Influence on reservoir quality. *J. Petrol. Geol.*, **25**, 297–324.

Hiscott, R.N. and **Middleton, G.V.** (1979) Depositional mechanics of thick-bedded sandstones at the base of a submarine slope, Tourelle Formation (Lower Ordovician), Quebec, Canada. In: *Geology of Continental Slopes* (Ed. Doyle, L.J. and Pilkey, O.H.), *SEPM, Spec. Publ.*, **27**, 307–326.

Hodgetts, D., **Drinkwater, N.J.**, **Hodgson, D.M.**, **Kavanagh, J.**, **Flint, S.S.**, **Keogh, K.J.** and **Howell, J.A.** (2004) Three-dimensional geological models from outcrop data using digital data collection techniques: an example from the Tanqua Karoo depocentre, South Africa. *Geol. Soc. London. Spec. Publ.*, **239**, 57–75.

Hodgson, D.M. (2009) Distribution and origin of hybrid beds in sand-rich submarine fans of the Tanqua depocentre, Karoo Basin, South Africa. *Mar. Petrol. Geol.*, **26**, 1940–1956.

Hodgson, D.M., **Flint, S.S.**, **Hodgetts, D.**, **Drinkwater, N.J.**, **Johannessen, E.P.** and **Luthi, S.M.** (2006) Stratigraphic evolution of fine-grained submarine fan systems, Tanqua Depocenter, Karoo Basin, South Africa. *J. Sed. Res.*, **76**, 20–40.

Hodgson, D.M., **Kane, I.A.**, **Flint, S.S.**, **Brunt, R.L.** and **Ortiz-karpf, A.** (2016) Time-transgressive confinement on the slope and the progradation of basin-floor fans: Implications for the sequence stratigraphy of deep-water deposits. *J. Sed. Res.*, **86**, 73–86.

Hofstra, M., **Pontén, A.S.M.**, **Peakall, J.**, **Flint, S.S.**, **Nair, K.N.** and **Hodgson, D.M.** (2017) The impact of fine-scale reservoir geometries on streamline flow patterns in submarine lobe deposits using outcrop analogues from the Karoo Basin. *Petrol. Geosci.*, **23**, 159–176.

Hubbard, S.M., **De Ruig, M.J.** and **Graham, S.A.** (2005) Utilizing outcrop analogs to improve subsurface mapping of natural gas-bearing strata in the Puchkirchen Formation, Molasse Basin, Upper Austria. *Austrian J. Earth Sci.*, **98**, 52–66.

Hubbard, S.M., **Covault, J.A.**, **Fildani, A.** and **Romans, B.W.** (2014) Sediment transfer and deposition in slope channels: Deciphering the record of enigmatic deep-sea processes from outcrop. *Geol. Soc. Am. Bull.*, **126**, 857–871.

Imran, J., **Islam, M.A.**, **Huang, H.**, **Kassem, A.**, **Dickerson, J.**, **Pirmez, C.** and **Parker, G.** (2007) Helical flow couplets in submarine gravity underflows. *Geology*, **35**, 659–662.

Jackson, A., **Stright, L.**, **Hubbard, S.M.** and **Romans, B.W.** (2019) Static connectivity of stacked deep-water channel elements constrained by high-resolution digital outcrop models. *AAPG Bull.*, **103**, 2943–2973.

Jobe, Z.R., **Bernhardt, A.** and **Lowe, D.R.** (2010) Facies and architectural asymmetry in a conglomerate-rich submarine channel fill, Cerro Toro Formation, Sierra Del Toro, Magallanes Basin, Chile. *J. Sed. Res.*, **80**, 1085–1108.

Jobe, Z.R., **Lowe, D.R.** and **Morris, W.R.** (2012) Climbing-ripple successions in turbidite systems: depositional environments, sedimentation rates and accumulation times. *Sedimentology*, **59**, 867–898.

Jobe, Z., **Sylvester, Z.**, **Pittaluga, M.B.**, **Frascati, A.**, **Pirmez, C.**, **Minisini, D.**, **Howes, N.** and **Cantelli, A.** (2017) Facies architecture of submarine channel deposits on the western Niger Delta slope: Implications for grain-size and density stratification in turbidity currents. *J. Geophys. Res. Earth Surf.*, **122**, 473–491.

Jobe, Z.R., **Howes, N.**, **Romans, B.W.** and **Covault, J.A.** (2018) Volume and recurrence of submarine fan building turbidity currents. *Depositional Rec.*, **4**, 160–176.

Johansson, M. and **Stow, D. A. V.** (1995) A classification scheme for shale clasts in deep water sandstones. In: *Characterization of Deep Marine Clastic Systems* (Ed. Hartley, A.J. and Prosser, D.J.), *Geol. Soc. London, Spec. Publ.*, **94**, 221–241.

Johnson, M.R., **Van Vuuren, C.J.**, **Hegenberger, W.F.**, **Key, R.** and **Show, U.** (1996) Stratigraphy of the Karoo Supergroup in southern Africa: an overview. *J. Afr. Earth Sci.*, **23**, 3–15.

Johnson, S., **Flint, S.**, **Hinds, D.** and **Wickens, H.** (2001) Anatomy of basin floor to slope turbidite systems, Tanqua Karoo, South Africa: sedimentology, sequence stratigraphy and implications for subsurface. *Sedimentology*, **48**, 987–1023.

Kane, I.A. and **Clare, M.A.** (2019) Dispersion, Accumulation, and the Ultimate Fate of Microplastics in Deep-Marine Environments: A Review and Future Directions. *Front. Earth Sci.*, **7**, 80.

Kane, I.A. and **Hodgson, D.M.** (2011) Sedimentological criteria to differentiate submarine channel levee subenvironments: Exhumed examples from the Rosario Fm. (Upper Cretaceous) of Baja California, Mexico, and the Fort Brown Fm. (Permian), Karoo Basin, S. Africa. *Mar. Petrol. Geol.*, **28**, 807–823.

Kane, I.A. and **Pontén, A.S.M.** (2012) Submarine transitional flow deposits in the Paleogene Gulf of Mexico. *Geology*, **40**, 1119–1122.

Kane, I.A., **Dykstra, M.L.**, **Kneller, B.C.**, **Tremblay, S.** and **McCaffrey, W.D.** (2009) Architecture of a coarse-grained

channel-levée system: The Rosario Formation, Baja California, Mexico. *Sedimentology*, **56**, 2207–2234.

Kane, I.A., **McCaffrey, W.D.** and **Peakall, J.** (2010) On the origin of paleocurrent complexity within deep marine channel levees. *J. Sed. Res.*, **80**, 54–66.

Kane, I.A., **Pontén, A.S.M.**, **Vangdal, B.**, **Eggenhuisen, J.T.**, **Hodgson, D.M.** and **Spychala, Y.T.** (2017) The stratigraphic record and processes of turbidity current transformation across deep-marine lobes. *Sedimentology*, **64**, 1236–1273.

Keevil, G.M., **Peakall, J.**, **Best, J.L.** and **Amos, K.J.** (2006) Flow structure in sinuous submarine channels: Velocity and turbulence structure of an experimental submarine channel. *Mar. Geol.*, **229**, 241–257.

Kneller, B.C. (2003) The influence of flow parameters on turbidite slope channel architecture. *Mar. Petrol. Geol.*, **20**, 901–910.

Kneller, B. and **Branney, M.** (1995) Sustained high-density turbidity currents and the deposition of thick massive sands. *Sedimentology*, **42**, 607–616.

Kolla, V., **Bourges, Ph.**, **Urruty, J.-M.** and **Safa, P.** (2001) Evolution of Deep-Water Tertiary Sinuous Channels Offshore Angola (West Africa) and Implications for Reservoir Architecture. *AAPG Bull.*, **85**, 1373–1405.

Kuenen, P.H. (1966) Experimental turbidite lamination in a circular flume. *J. Geol.*, **74**, 523–545.

Labourdette, R. and **Bez, M.** (2010) Element migration in turbidite systems: Random or systematic depositional processes? *AAPG Bull.*, **94**, 345–368.

Larue, D.K. and **Hovadik, J.** (2006) Connectivity of channelized reservoirs: a modelling approach. *Petrol. Geosci.*, **12**, 291–308.

Leclair, S.F. and **Arnott, R.W.C.** (2005) Parallel lamination formed by high-density turbidity currents. *J. Sed. Res.*, **75**, 1–5.

Li, P., **Kneller, B.C.**, **Hansen, L.** and **Kane, I.A.** (2016) The classical turbidite outcrop at San Clemente, California revisited: An example of sandy submarine channels with asymmetric facies architecture. *Sed. Geol.*, **346**, 1–16.

Lien, T., **Midtbø, R.E.** and **Martinsen, O.J.** (2006) Depositional facies and reservoir quality of deep-marine sandstones in the Norwegian Sea. *Nor. J. Geol.*, **86**, 71–92.

Lowe, D.R. (1975) Water escape structures in coarse-grained sediments. *Sedimentology*, **22**, 157–204.

Lowe, D.R. (1982) Sediment gravity flows:II depositional models with special reference to the deposits of high-density turbidity currents. *J. Sed. Res.*, **52**, 279–297.

Lowe, D.R. (1988) Suspended-load fallout rate as an independent variable in the analysis of current structures. *Sedimentology*, **35**, 765–776.

Macauley, R.V. and **Hubbard, S.M.** (2013) Slope channel sedimentary processes and stratigraphic stacking, Cretaceous Tres Pasos Formation slope system, Chilean Patagonia. *Mar. Petrol. Geol.*, **41**, 146–162.

Malkowski, M.A., **Jobe, Z.R.**, **Sharman, G.R.** and **Graham, S.A.** (2018) Down-slope facies variability within deep-water channel systems: Insights from the Upper Cretaceous Cerro Toro Formation, southern Patagonia. *Sedimentology*, **65**, 1918–1946.

Mayall, M., **Jones, E.** and **Casey, M.** (2006) Turbidite channel reservoirs—Key elements in facies prediction and effective development. *Mar. Petrol. Geol.*, **23**, 821–841.

McCaffrey, W. and **Kneller, B.** (2001) Process controls on the development of stratigraphic trap potential on the margins of confined turbidite systems and aids to reservoir evaluation. *AAPG Bull.*, **85**, 971–988.

McHargue, T., **Pyrcz, M.J.**, **Sullivan, M.D.**, **Clark, J.D.**, **Fildani, A.**, **Romans, B.W.**, **Covault, J.A.**, **Levy, M.**, **Posamentier, H.W.** and **Drinkwater, N.J.** (2011) Architecture of turbidite channel systems on the continental slope: Patterns and predictions. *Mar. Petrol. Geol.*, **28**, 728–743.

Milliman, J.D. and **Syvitski, J.P.M.** (1992) Geomorphic/tectonic control of sediment discharge to the ocean: The importance of small mountainous rivers. *J. Geol.*, **100**, 525–544.

Moody, J.D., **Pyles, D.R.**, **Clark, J.** and **Bouroullec, R.** (2012) Quantitative outcrop characterization of an analog to weakly confined submarine channel systems: Morillo 1 member, Ainsa Basin, Spain. *AAPG Bull.*, **96**, 1813–1841.

Morris, E.A., **Hodgson, D.M.**, **Brunt, R.L.** and **Flint, S.S.** (2014) Origin, evolution and anatomy of silt-prone submarine external levées. *Sedimentology*, **61**, 1734–1763.

Morris, E.A., **Hodgson, D.M.**, **Flint, S.**, **Brunt, R.L.**, **Luthi, S.M.** and **Kolenberg, Y.** (2016) Integrating outcrop and subsurface data to assess the temporal evolution of a submarine channel-levee system. *AAPG Bull.*, **100**, 1663–1691.

Mutti, E. (1977) Distinctive thin-bedded turbidite facies and related depositional environments in the Eocene Hecho Group (South-central Pyrenees, Spain). *Sedimentology*, **24**, 107–131.

Mutti, E. (1984) The Hecho Eocene submarine fan system, south-central Pyrenees, Spain. *Geo-Mar. Lett.*, **3**, 199–202.

Mutti, E. (1992) *Turbidite Sandstones*. Agip, Istituto di Geologia Università di Parma, Milan, 1–256 pp.

Mutti, E. and **Normark, W.R.** (1987) Comparing examples of modern and ancient turbidite systems: problems and concepts. In: *Marine Clastic Sedimentology* (Eds Leggett, J.K. and Zuffa, G.G.), pp. 1–38. Springer Netherlands, Dordrecht.

Mutti, E. and **Ricci Lucchi, F.** (1978) Turbidites of the northern Apennines: introduction to facies analysis. *Int. Geol. Rev.*, **20**, 125–166.

Navarro, L., **Khan, Z.** and **Arnott, R.W.C.** (2007) Depositional architecture and evolution of a deep-marine channel-levee complex: Isaac Formation (Windermere Supergroup), Southern Canadian Cordiller. In: *Atlas of deep-water outcrops*, *AAPG Studies in Geology 56, CD-ROM*, 22 p.

Newport, S.M., **Jerrett, R.M.**, **Taylor, K.G.**, **Hough, E.** and **Worden, R.H.** (2017) Sedimentology and microfacies of a mud-rich slope succession: in the Carboniferous Bowland Basin, NW England (UK). *J. Geol. Soc. London*, **175**, 247–262.

Peakall, J. and **Sumner, E.J.** (2015) Submarine channel flow processes and deposits: A process-product perspective. *Geomorphology*, **244**, 95–120.

Peakall, J., **Amos, K.J.**, **Keevil, G.M.**, **William Bradbury, P.** and **Gupta, S.** (2007) Flow processes and sedimentation in submarine channel bends. *Mar. Petrol. Geol.*, **24**, 470–486.

Pickering, K.T. and **Bayliss, N.J.** (2009) Deconvolving tectono-climatic signals in deep-marine siliciclastics, Eocene Ainsa basin, Spanish Pyrenees: Seesaw tectonics versus eustasy. *Geology*, **37**, 203–206.

Pickering, K.T. and **Corregidor, J.** (2005) Mass-transport complexes, (MTCs) and tectonic control on basin-floor submarine fans, middle eocene, south Spanish Pyrenees. *J. Sed. Res.*, **75**, 761–783.

Pierce, C.S., **Haughton, P.D.**, **Shannon, P.M.**, **Pulham, A.J.**, **Barker, S.P.** and **Martinsen, O.J.** (2018) Variable character

and diverse origin of hybrid event beds in a sandy submarine fan system, Pennsylvanian Ross Sandstone Formation, western Ireland. *Sedimentology*, **65**, 952–992.

Piper, D.J.W. (1972) Turbidite origin of some laminated mudstones. *Geol. Mag.*, **109**, 115–126.

Piper, D.J.W. and **Aksu, A.E.** (1987) The source and origin of the 1929 Grand Banks turbidity current inferred from sediment budgets. *Geo-Mar. Lett.*, **7**, 177–182.

Pitts, A.D., **Casciano, C.I.**, **Patacci, M.**, **Longhitano, S.G.**, **Di Celma, C.** and **McCaffrey, W.D.** (2017) Integrating traditional field methods with emerging digital techniques for enhanced outcrop analysis of deep water channel-fill deposits. *Mar. Petrol. Geol.*, **87**, 2–13.

Porten, K.W., **Kane, I.A.**, **Warchol, M.** and **Southern, S.J.** (2016) Depositional reservoir quality of deep-marine sandstones: A sedimentolgical process-based approach - an example from the Springrar Formation, North-Western Vøring Basin, Norwegian Sea. *J. Sed. Res.*, **86**, 1269–1286.

Poyatos-Moré, M., **Jones, G.D.**, **Brunt, R.L.**, **Hodgson, D.M.**, **Wild, R.J.** and **Flint, S.S.** (2016) Mud-dominated basin-margin progradation: processes and implications. *J. Sed. Res.*, **86**, 863–878.

Prather, B.E. (2003) Controls on reservoir distribution, architecture and stratigraphic trapping in slope settings. *Mar. Petrol. Geol.*, **20**, 529–545.

Prélat, A., **Hodgson, D.M.** and **Flint, S.S.** (2009) Evolution, architecture and hierarchy of distributary deep-water deposits: a high-resolution outcrop investigation from the Permian Karoo Basin, South Africa. *Sedimentology*, **56**, 2132–2154.

Prélat, A., **Covault, J.A.**, **Hodgson, D.M.**, **Fildani, A.** and **Flint, S.S.** (2010) Intrinsic controls on the range of volumes, morphologies, and dimensions of submarine lobes. *Sed. Geol.*, **232**, 66–76.

Pyles, D.R., **Jennette, D.C.**, **Tomasso, M.**, **Beaubouef, R.T.** and **Rossen, C.** (2010) Concepts learned from a 3D outcrop of a sinuous slope channel complex: Beacon Channel Complex, Brushy Canyon Formation, West Texas, U.S.A. *J. Sed. Res.*, **80**, 67–96.

Pyles, D.R., **Tomasso, M.** and **Jennette, D.C.** (2012) Flow processes and sedimentation associated with erosion and filling of sinuous submarine channels. *Geology*, **40**, 143–146.

Reading, H.G. and **Richards, M.** (1994) Turbidite systems in deep-water basin margins classified by grain size and feeder system. *AAPG Bull.*, **78**, 792–822.

Reimchen, A.P., **Hubbard, S.M.**, **Stright, L.** and **Romans, B.W.** (2016) Using sea-floor morphometrics to constrain stratigraphic models of sinuous submarine channel systems. *Mar. Petrol. Geol.*, **77**, 92–115.

Schwarz, E. and **Arnott, R.W.C.** (2007) Anatomy and evolution of a slope channel-complex set (Neoproterozoic Isaac Formation, Windermere Supergroup, Southern Canadian Cordillera): Implications for reservoir characterization. *J. Sed. Res.*, **77**, 89–109.

Scotchman, J.I., **Pickering, K.T.**, **Sutcliffe, C.**, **Dakin, N.** and **Armstrong, E.** (2015) Milankovitch cyclicity within the middle Eocene deep-marine Guaso System, Ainsa Basin, Spanish Pyrenees. *Earth-Sci. Rev.*, **144**, 107–121.

Shanmugam, G. (1996) High-density turbidity currents; are they sandy debris flows? *J. Sed. Res.*, **66**, 2–10.

Smith, R.M.H. (1990) A review of stratigraphy and sedimentary environments of the Karoo Basin of South Africa. *J. Afr. Earth Sci.*, **10**, 117–137.

Sohn, Y.K. (1997) On traction-carpet sedimentation. *J. Sed. Res.*, **67**, 502–509.

Sømme, T.O., **Helland-Hansen, W.**, **Martinsen, O.J.** and **Thurmond, J.B.** (2009) Relationships between morphological and sedimentological parameters in source-to-sink systems: a basis for predicting semi-quantitative characteristics in subsurface systems. *Basin Res.*, **21**, 361–387.

Sorby, H.C. (1908) On the application of quantitative methods to the study of the structure and history of rocks. *Q. J. Geol. Soc. London*, **64**, 171–233.

Southard, J.B. (1991) Experimental determination of bed-form stability. *Annu. Rev. Earth Planet. Sci.*, **19**, 423–455.

Southern, S.J., **Patacci, M.**, **Felletti, F.** and **Mccaffrey, W.D.** (2015) Influence of flow containment and substrate entrainment upon sandy hybrid event beds containing a co-genetic mud-clast-rich division. *Sed. Geol.*, **321**, 105–122.

Sprague, A.R., **Sullivan, M.D.**, **Campion, K.M.**, **Jensen, G.N.**, **Goulding, F.J.**, **Garfield, T.R.**, **Sickafoose, D.K.**, **Rossen, C.** and **Jeannette, D.C.** (2002) The physical stratigraphy of deep-water strata: A hierarchical approach to the analysis of genetically-related stratigraphic elements for improved reservoir prediction. *National AAPG/SEPM Meeting Abstracts*, Houston, TX, 10–13.

Sprague, A.R., **Garfield, T.R.**, **Goulding, F.J.**, **Beaubouef, R.T.**, **Sullivan, M.D.**, **Rossen, C.**, **Campion, K.M.**, **Sickafoose, D.K.**, **Abreu, V.**, **Schellpeper, M.E.**, **Jensen, G.N.**, **Jennette, D.C.**, **Pirmez, C.**, **Dixon, B.T.**, **Ying, D.**, **Ardill, J.**, **Mohrig, D.C.**, **Porter, M.L.**, **Farrell, M.E.** and **Mellere, D.** (2005) Integrated slope channel depositional models: the key to successful prediction of reservoir presence and quality in offshore West Africa. In: CIPM, cuarto EExitep 2005, Veracruz, Mexico, 17, 1–13.

Spychala, Y.T., **Hodgson, D.M.**, **Prélat, A.**, **Kane, I.A.**, **Flint, S.S.** and **Mountney, N.P.** (2017) Frontal and lateral submarine lobe fringes: Comparing facies, architecture and flow processes. *J. Sed. Res.*, **87**, 1–21.

Stelting, C.E., **Bouma, A.H.** and **Stone, C.G.** (2000) Fine-grained turbidite systems: Overview. In: *Fine-Grained Turbidite Systems* (Eds. Bouma, A.H. and Stone, C.G.), *AAPG Mem. 72:SEPM Spec. Publ.*, 1–7.

Stevenson, C.J., **Jackson, C.A.-L.**, **Hodgson, D.M.**, **Hubbard, S.M.** and **Eggenhuisen, J.T.** (2015) Deep-water sediment bypass. *J. Sed. Res.*, **85**, 1058–1081.

Stow, D.A.V. and **Bowen, A.J.** (1980) A physical model for the transport and sorting of fine-grained sediment by turbidity currents. *Sedimentology*, **27**, 31–46.

Stright, L., **Stewart, J.**, **Campion, K.** and **Graham, S.** (2014) Geologic and seismic modeling of a coarse-grained deep-water channel reservoir analog (Black's Beach, La Jolla, California). *AAPG Bull.*, **98**, 695–728.

Sullivan, M.D., **Jensen, G.N.**, **Goulding, F.J.**, **Jennette, D.C.**, **Foreman, J.L.** and **Stern, D.** (2000) Architectural analysis of deep-water outcrops: Implications for exploration and development of the Diana sub-basin, western Gulf of Mexico. In: *Deep-Water Reservoirs of the World* (Eds. Weimer, P., Slatt, R.M., Bouma, A.H. and Lawrence, D.T.), *Gulf Coast Section SEPM Foundation, Twentieth Annual Research Conference*, 1010–1032.

Sumner, E.J., **Amy, L.A.** and **Talling, P.J.** (2008) Deposit structure and processes of sand deposition from decelerating sediment suspensions. *J. Sed. Res.*, **78**, 529–547.

Sumner, E.J., **Talling, P.J.**, **Amy, L.A.**, **Wynn, R.B.**, **Stevenson, C.J.** and **Frenz, M.** (2012) Facies architecture of

individual basin-plain turbidites: Comparison with existing models and implications for flow processes. *Sedimentology*, **59**, 1850–1887.

Sylvester, Z. and **Lowe, D.R.** (2004) Textural trends in turbidites and slurry beds from the Oligocene flysch of the East Carpathians, Romania. *Sedimentology*, **51**, 945–972.

Sylvester, Z., **Pirmez, C.** and **Cantelli, A.** (2011) A model of submarine channel-levee evolution based on channel trajectories: Implications for stratigraphic architecture. *Mar. Petrol. Geol.*, **28**, 716–727.

Talling, P.J., **Wynn, R.B.**, **Masson, D.G.**, **Frenz, M.**, **Cronin, B.T.**, **Schiebel, R.**, **Akhmetzhanov, A.M.**, **Dallmeier-Tiessen, S.**, **Benetti, S.**, **Weaver, P.P.E.**, **Georgiopoulou, A.**, **Zühlsdorff, C.** and **Amy, L.A.** (2007) Onset of submarine debris flow deposition far from original giant landslide. *Nature*, **450**, 541–544.

Talling, P.J., **Masson, D.G.**, **Sumner, E.J.** and **Malgesini, G.** (2012) Subaqueous sediment density flows: Depositional processes and deposit types. *Sedimentology*, **59**, 1937–2003.

Talling, P.J., **Malgesini, G.** and **Felletti, F.** (2013) Can liquefied debris flows deposit clean sand over large areas of sea floor? Field evidence from the Marnoso-arenacea Formation, Italian Apennines. *Sedimentology*, **60**, 720–762.

Veevers, J.J., **Cole, D.I.** and **Cowan, E.J.** (1994) Southern Africa: Karoo Basin and Cape Fold Belt. In: *Permian-Triassic Pangean Basins and Foldbelts Along the Panthalassan Margin of Gondwanaland* (Eds. Veevers, J.J. and Powell, C.M.), *Mem. Geol. Soc. Am.*, **184**, 223–279.

Vendettuoli, D., **Clare, M.A.**, **Hughes Clarke, J.E.**, **Vellinga, A.**, **Hizzet, J.**, **Hage, S.**, **Cartigny, M.J.B.**, **Talling, P.J.**, **Waltham, D.**, **Hubbard, S.M.**, **Stacey, C.** and **Lintern, D.G.** (2019) Daily bathymetric surveys document how stratigraphy is built and its extreme incompleteness in submarine channels. *Earth Planet. Sci. Lett.*, **515**, 231–247.

Viglietti, P.A., **Rubidge, B.S.** and **Smith, R.M.H.** (2017) New Late Permian tectonic model for South Africa's Karoo Basin: foreland tectonics and climate change before the end-Permian crisis. *Sci. Rep.*, **7**, 10861.

Visser, J.N.J. (1994) A Permian argillaceous syn- to post-glacial foreland sequence in the Karoo Basin, South Africa. In: *Earth's Glacial Record* (Eds Deynoux, M., Miller, G., Domack, E.W., Eyles, N., Fairchild, I. and Young, G.M.), pp. 193–203. Cambridge University Press, Cambridge.

Visser, J.N.J. and **Praekelt, H.E.** (1996) Subduction, mega-shear systems and Late Palaeozoic basin development in the African segment of Gondwana. *Geol. Rundsch.*, **85**, 632–646.

Walker, R.G. (1965) The origin and significance of the internal sedimentary structures of turbidites. *Proc. Yorks. Geol. Soc.*, **35**, 1–32.

Walker, R.G. (1966a) Shale Grit and Grindslow shales; transition from turbidite to shallow water sediments in the upper Carboniferous of northern England. *J. Sed. Res.*, **36**, 90–114.

Walker, R.G. (1966b) Deep channels in turbidite-bearing formations. *AAPG Bull.*, **50**, 1899–1917.

Walker, R.G. (1975) Nested submarine-fan channels in the Capistrano Formation, San Clemente, California. *Geol. Soc. Am. Bull.*, **86**, 915–924.

Wang, Z. and **Larsen, P.** (1994) Turbulent Structure of Water and Clay Suspensions with Bed Load. *J. Hydraul. Eng.*, **120**, 577–600.

Weimer, P., **Slatt, R.M.**, **Dromgoole, P.**, **Bowman, M.** and **Leonard, A.** (2000) Developing and managing turbidite reservoirs: Case histories and experiences : Results of the 1998 EAGE/AAPG Research Conference 1. *AAPG Bull.*, **84**, 453–465.

Wickens, H. de V. (1994) Basin floor fan building turbidites of the southwestern Karoo Basin, Permian Ecca Group, South Africa. PhD Thesis, University of Port Elizabeth, 223p.

Wild, R.J., **Hodgson, D.M.** and **Flint, S.S.** (2005) Architecture and stratigraphic evolution of multiple, vertically-stacked slope channel complexes, Tanqua depocentre, Karoo Basin, South Africa. *Geol. Soc. London. Spec. Publ.*, **244**, 89–111.

Wild, R., **Flint, S.S.** and **Hodgson, D.M.** (2009) Stratigraphic evolution of the upper slope and shelf edge in the Karoo Basin, South Africa. *Basin Res.*, **21**, 502–527.

Zhang, J., **Wu, S.**, **Wang, X.**, **Lin, Y.**, **Fan, H.**, **Jiang, L.**, **Wan, Q.**, **Yin, H.** and **Lu, Y.** (2015) Reservoir quality variations within a sinuous deep water channel system in the Niger Delta Basin, offshore West Africa. *Mar. Petrol. Geol.*, **63**, 166–188.

Manuscript received 15 July 2019; revision accepted 8 April 2020